Chapter I.14

Accelerator design workshop

Bastian Härer [a], *Adrian Oeftiger* [b,c]

[a] Karlsruhe Institute of Technology, Karlsruhe, Germany

[b] University of Oxford, Oxford, United Kingdom

[c] GSI Helmholtz Centre for Heavy Ion Research, Darmstadt, Germany

After studying the relevant aspects of accelerators topic by topic, it is time to gain hands-on experience by designing a realistic particle accelerator. This chapter describes the accelerator design workshop which takes place at the end of JUAS course I. The core idea is to gain experience how such a large task can be split up and organised into collaborating teams with different expertise, with a particular focus on how certain design decisions affect everything else. In a collaborative effort, several teams participate in a top factory study tackling the design of a high-energy collider. The teams approach the design from three complementary angles viz., the *general parameters* teams determine a basic beam and machine parameter set, the *RF* teams design the radio-frequency systems with respect to acceleration and synchrotron radiation, and the *lattice design* teams work out an accelerator lattice using the `MAD-X` suite. The teams require inputs from the respective other topics to complete their tasks. During the workshop conclusion following the oral group examinations, selected teams present their results in a conference style setting. This approach sets the scene for a motivating, competitive and fun workshop event while fostering participants to understand the mutual dependencies between accelerator and beam parameters and the implications of design decisions, involving the knowledge they gained during the JUAS school.

I.14.1 Workshop philosophy

The goal of the accelerator design workshop is to apply the knowledge gained during the JUAS school to a realistic case study. The task is to design a particle accelerator with certain specifications and boundary conditions. The idea is to gain experience how such a large task is tackled and organised. This is the time during the JUAS school where the workshop participants patch together the specific knowledge from all the previously covered topics, understanding the links between them and the corresponding impact of design decisions on various accelerator parameters. The workshop format is set up such that teams of participants work together in collaboration. The case study is approached from three different sides, and teams are assigned to represent an expert group for one of these corresponding three focus topics. Before the teams start into the group work phase, a dedicated accelerator design lecture summarises and gathers the most relevant information from previous lectures and offers practical design considerations.

Based on the experience from the JUAS schools where this workshop was taught, a team size of three participants turns out to be ideal for close collaboration within the teams. This choice balances the work load and, thus, spreads the knowledge gain as evenly as possible across all workshop participants.

This chapter should be cited as: Accelerator design workshop, B. Härer and A. Oeftiger, DOI: 10.23730/CYRSP-2024-003.661, in: Proceedings of the Joint Universities Accelerator School (JUAS): Courses and exercises, E. Métral (ed.), CERN Yellow Reports: School Proceedings, CERN-2024-003, DOI: 10.23730/CYRSP-2024-003, p. 661.

Choosing more participants per team was observed to result in single participants taking a more inactive and passive role, while choosing teams of only two participants sometimes limited their creative potential and more input was required from the tutor side to spark ideas.

The three focus topics *general parameters*, *RF design* and *lattice design* touch on most of the JUAS course I topics. There is a set of open exercises for each topic (see the appendix to this chapter), along which a corresponding team will work out their accelerator design. The lattice design tasks are implemented in a fill-the-gap interactive python notebook [1]. For typical JUAS attendance numbers there are around two to four teams per focus topic. As they work through the same exercise set per topic, the teams of a given topic compete to work out the most well-founded design. The exercises are kept open such that different answers may be formally correct, and the participants are required to justify their choices. The competitive aspect of the workshop is observed to stimulate the motivation of participants. Some exercises are designed such that the teams require input from the other topics: these links between the topics represent the interaction between research teams in real design studies.[1] These inter-topical discussions are observed to take a key role in achieving the goals of the workshop, which are being instructive and triggering the understanding of intertwined beam and accelerator parameters. Different priorities of topical goals lead to individual design choices taken by each team. In other words, rather than aiming for single correct results, the exercises demand the teams to develop a well argued motivation behind their choice.

In order to render the workshop experience more realistic and interesting, the case study chosen here evolves around a real project instead of an entirely hypothetical machine. The teams collaboratively design a top factory aligned closely with the parameters of the lepton version of the Future Circular Collider (FCC-ee), and they discuss and decide on optimal parameter sets. In contrast to classical tutoring where tutors instruct and actively guide the learning process, the role of the tutors here is to support and complement the design process within the teams during the main part of the workshop, just like a senior colleague or consultant would do. During the oral examination then, the tutors "switch sides" and can be thought of to represent a political committee: they need to decide on the best design per topic which has been presented in the most convincing way and, thus, "deserves full funding". A corresponding presentation of selected results by the best teams at the end of the workshop along with a general plenary discussion rounds up the process of understanding for the participants.

This chapter is presented in a style intending to reflect the workshop atmosphere and the discussions between the workshop participants and the tutors. Typical questions and corresponding possible discussions from the team work phase complement the presented story line of the case study, including all the lecture contents.

[1] Practical observations: in the online JUAS format, the teams were working separately in breakout rooms and could briefly join teams from other topics for the discussions. At least two links per topic between the exercise sets were required to keep alive a running discussion between the topics. For the on-site JUAS format at ESI, the teams worked in workshop rooms, as nearby located as possible. Very active and lively discussions were observed already with one or two links per topic. More than two exercises linking to other topics are likely to inhibit effective group work. Throughout the workshop, teams are likely to change their design decisions to work out a more coherent design, and correspondingly the input given to other teams might become obsolete. Within the scope of the JUAS accelerator design workshop, teams are encouraged to ignore this fact and just continue their design focusing on the original input. During the oral examination, these inputs from other teams were not taken into account for the evaluation (unless they were obviously questionable). Given the limited time during the JUAS, the teams were explicitly not obliged to converge on a single set of parameters for the case study.

I.14.2 What does accelerator design actually mean?

The design of an accelerator typically orients itself along an experimental request, e.g. the production of top-antitop quark pairs. Those experimental requests have to be translated into accelerator requirements, in this case maximising the production rate leads to certain request on required kinetic energy and luminosity. Once a basic parameter set is defined, several aspects have to be covered: first, the type of particle beam (protons, electrons, ...) and the accelerator type (cyclotron, linear accelerator, synchrotron, ...) need to be identified. Then the lattice is designed, transverse and longitudinal beam dynamics are optimised and potentially limiting instabilities are addressed. The next step considers the hardware requirements (magnets, RF systems, beam instrumentation, ...), which often results in adjustments of the previous decisions. In the final part, engineering challenges are investigated and solved (civil engineering, power concepts, surveying, ...). Usually, such a design requires an iterative approach. Lattice and optics have to be adapted according to technical requirements and vice versa.

The accelerator design workshop focuses on the first two stages. The introductory lectures break down the design process of a high-energy collider and present a step-by-step approach:

Step I: Decide on the particle species, beam energy and general layout.

Step II: Calculate the beam rigidity and the required bending fields.

Step III: Determine the focusing structure and calculate the beam optics.

Step IV: Determine synchrotron radiation losses, specify the RF system and the space needed.

Step V: Open the arc lattice and install dispersion suppressors for dispersion-free straight sections.

Step VI: Include matching sections if needed.

Step VII: Install interaction regions.

We follow this sensible guideline. Let's start designing an accelerator!

I.14.3 Step I: General layout, particle species and beam energy

Determine particle type and beam energy suited for the specific experiment. Define the general layout of the accelerator.

This section covers basic considerations which are usually consequences of the experimental requests and/or user requirements: What kind of particles should be accelerated, and to what energy? What collision layout is foreseen and what collider geometry is chosen?

I.14.3.1 What particle species should we choose for our accelerator?

The choice of the particle species depends on the application of the beams. In the case of high-energy physics both hadrons and electrons/positrons are used. As the name says, high-energy storage rings aim for particle beams with highest possible beam energy, which will then be collided to study the

fundamental physics of the standard model and beyond. Hadrons, such as protons or heavy ions, carry more mass than electrons or positrons. As a consequence, using hadron beams makes it easier to reach higher centre-of-mass energies as the emission of synchrotron radiation is usually (below $\sim$ 1 TeV) suppressed due to the large mass. **Hadron colliders are therefore used as discovery machines**. They push on the energy frontier and explore for new, unknown particles.

However, hadrons are composite particles. For instance, the proton comprises three valence quarks along with a sea of virtual particles such as gluons, quarks and antiquarks. Each of these elementary particles carries only a fraction of the proton's total momentum. In the event of a collision with one of these elementary particles, not all the kinetic energy of the composite proton is available for creating new particles in the collision process. This results in a significantly wider distribution of generated particles, which leads to a large background of "non-interesting" collision products. Figure I.14.1a depicts such a hadron collision event from the CMS detector at the CERN LHC (Large Hadron Collider), where a lot of traces from collision products need to be resolved.

In this sense, the big advantage of leptons is that they are elementary particles. During a collision of an electron and a positron, two particles are involved with well-defined momenta giving a well-defined centre-of-mass energy. Therefore, electron-positron colliders provide cleaner results in the collision process, i.e., background as described for hadron beam collisions is strongly suppressed and the collision products are well defined with respect to the provided kinetic energy of the primary particle beam. Figure I.14.1b shows such a collision event recorded by the detector OPAL at the LEP (Large Electron-Positron) collider. **Lepton colliders are, therefore, typically used for targeted precision measurements**.

On the other hand, the beam dynamics is heavily driven by the emission of synchrotron radiation. As the mass of electrons and positrons ($m_\mathrm{e} = 0.511\,\mathrm{MeV/c^2}$) is nearly 2000 times smaller than the mass of a proton ($m_\mathrm{p} = 938\,\mathrm{MeV/c^2}$), the Lorentz factor of an electron γ_e becomes orders of magnitude larger compared to the Lorentz factor of a proton γ_p with the same energy

$$\begin{aligned} E = 10\,\mathrm{GeV} \quad &\rightarrow \gamma_\mathrm{p} = 11 \\ &\rightarrow \gamma_\mathrm{e} = 19570. \end{aligned}$$

Since the emitted synchrotron radiation power is proportional to the fourth power of the Lorentz factor, synchrotron radiation becomes a critical factor for high-energy electron/positron storage rings.

Question I.14.1: Based on the discussion above, can you explain why a circular muon collider is an attractive alternative?

Question I.14.2: The Large Electron Positron Collider (LEP) was a single-ring collider, which means both beams shared on vacuum chamber. The Large Hadron Collider (LHC) on the other hand is a double-ring collider, in which the two beams have their individual beam pipes. Why was it not possible to realize LHC as a single-ring collider? What does a single-ring collider entail?

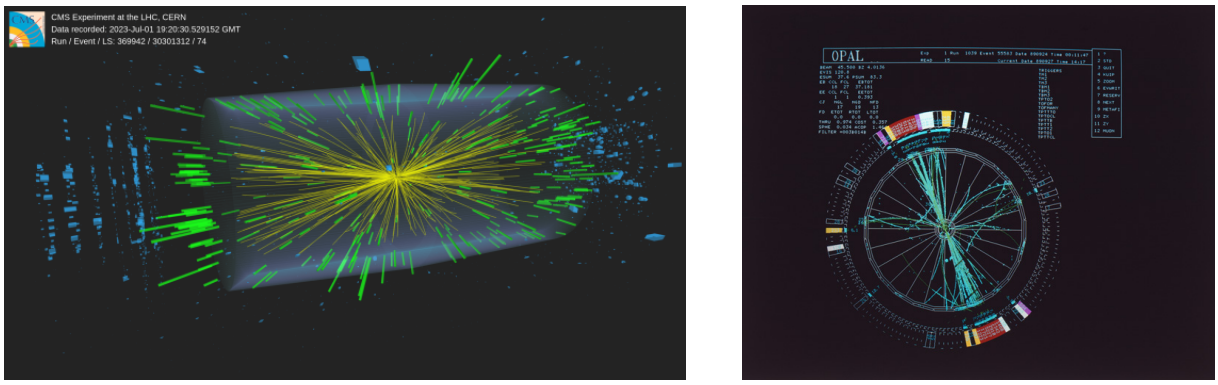

(a) **(b)**

Fig. I.14.1: Comparison of collision events in hadron and electron-positron colliders: (a) shows an event in CMS at the hadron collider LHC [2] and (b) displays an OPAL event at the electron-positron collider LEP [3].

I.14.3.2 What is the difference between fixed-target and collider geometry?

There are two possible geometries for particle collisions: let us first consider the Rutherford experiment, where a gold foil was bombarded by a beam consisting of alpha particles. This layout is a typical fixed-target experiment, in which the sample at a fixed position is probed by a beam of particles. This arrangement offers high event rates, since the target, often a solid body, has a high particle density.

In the context of high-energy physics, the decisive factor for excitation of higher energy states or the production of new particles is the centre-of-mass energy $\sqrt{s}$. Given the four-vector momenta p_1 and p_2 of the two colliding particles and using natural units where $c = 1$,

$$s = (p_1 + p_2)^2 = p_1^2 + p_2^2 + 2p_1p_2 = m_1^2 + m_2^2 + 2\left(E_1E_2 - \vec{p}_1\vec{p}_2\right). \tag{I.14.1}$$

In fixed-target geometry we have $\vec{p}_2 = \vec{0}$ and $E_2 = m_2$. The centre-of-mass energy then reads

$$\sqrt{s} = \sqrt{m_1^2 + m_2^2 + 2E_1m_2} \propto \sqrt{E_1}. \tag{I.14.2}$$

As a consequence, the energy reach at high energies ($E_1 \gg m_1, m_2$) is limited, as the centre-of-mass energy is proportional only to the square root of the beam energy E_1.

An approach to mitigate this limitation is to collide two particle beams instead, which are both simultaneously used as target and probing beam. Assuming the collision of particles with same mass ($m_1 = m_2 = m$) and energy ($\vec{p}_1 = -\vec{p}_2$), the centre-of-mass energy in the collider geometry is

$$\sqrt{s} = \sqrt{2m^2 + 2E^2 + 2|\vec{p}|^2} = 2E \propto E. \tag{I.14.3}$$

The drawback of this geometry is the low event rate resulting from the low particle density in the collided beams.

Question I.14.3: You would like to conduct an experiment, for which you need a centre-of-mass energy of $\sqrt{s} = 200\,\mathrm{GeV}$. Calculate the beam energy you need if you collide two proton beams. Next, consider a single proton beam and a fixed hydrogen target. What beam energy is now required?

I.14.3.3 What defines the beam energy of our accelerator?

In the case of exploratory hadron colliders, the energy shall be pushed as high as possible. As the beam energy (or particle momentum p_0) is determined by the integrated magnetic field B (see also Sec. I.14.4.2),

$$2\pi\frac{p_0}{e} = \oint B\,\mathrm{d}s, \tag{I.14.4}$$

the beam energy is finally limited by technical constraints such as the maximum achievable magnetic field of the (superconducting) magnets, the maximum circumference etc. As such projects require long-term planning and preparation over a duration of decades, it is reasonable to take into account expected results of future technical research and development (R&D) during the design process.

Precision machines on the other hand target certain events or particles to be produced such as, for example, the Higgs boson. The beam energy in this case is determined by the cross-section depending on the centre-of-mass energy. The cross-section shows either a resonance as in the case of the Z boson, which is displayed in Fig. I.14.2a, or an energy threshold as for the the Higgs boson, which is depicted in Fig. I.14.2b. These cross-sections define the operation modes and corresponding beam energies for which precision machines are optimised for. In the example case of the FCC-ee, four operation modes are foreseen: Z production with a beam energy of $45.6\,\mathrm{GeV}$, W production at $80\,\mathrm{GeV}$, Higgs production at $120\,\mathrm{GeV}$, and $t\bar{t}$ pair production at $182.5\,\mathrm{GeV}$.

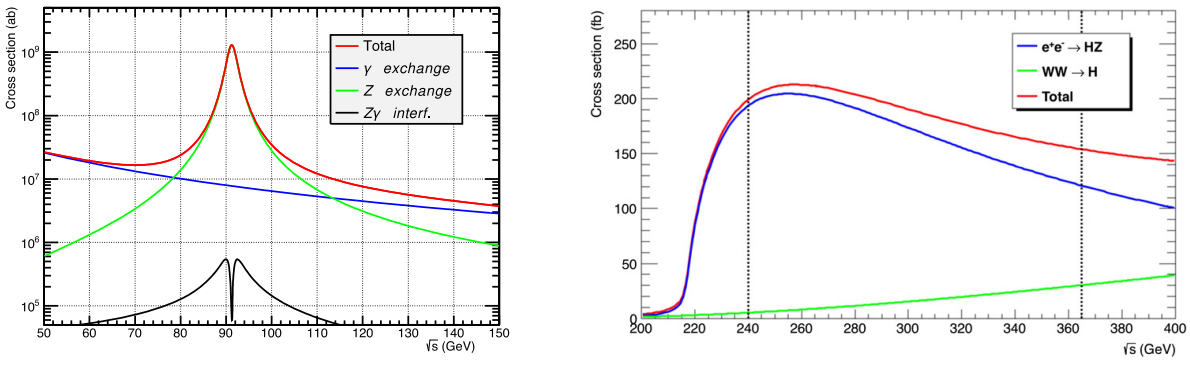

(a) **(b)**

Fig. I.14.2: Cross-section of the Z and Higgs production in electron-positron collisions [4]. The Z cross-section has a resonance shape, the Higgs cross-sections shows a production threshold.

I.14.3.4 Why are there linear and circular colliders?

Linear colliders are proposed in the context of high-energy electron-positron collisions. As mentioned above, the synchrotron radiation power P_γ is proportional to γ^4 (see Chapter I.10 on synchrotron radiation). As a consequence, for collision energies beyond a threshold of about $500\,\mathrm{GeV}$ the synchrotron radiation power becomes unbearable in terms of energy efficiency and equipment shielding unless the collider reached an enormous size beyond hundreds of kilometers. Linear colliders have been proposed to resolve this issue. Since the particle beams are not deflected onto a ring geometry here, no synchrotron radiation is emitted and higher beam energies can in principle be reached. However, the geometry of a linear collider allows for only one experiment to take data at a given time, whereas circular colliders typically feature several experiments at several interaction points running simultaneously. Also, it has to be kept in mind, that only ≈ 10 collisions take place during one bunch crossing. In linear collider the rest of the $\approx 10^{11}$ particles go to the dump at their full kinetic energy, while in a circular collider they get the chance to collide again after one turn or in the next experiment. Due to this recycling effect, circular colliders are preferred at energies below $500\,\mathrm{GeV}$ centre-of-mass energy as they reach much higher luminosities (see Sections I.14.10.1 and I.14.10.2). In the end, the choice of linear or circular collider geometry is the result of a trade-off between expected synchrotron radiation power and luminosity reach. Figure I.14.3 compares the expected instantaneous luminosities of potential future electron-positron colliders. At energies below $300\,\mathrm{GeV}$ the circular collider projects FCC-ee (Future Circular Collider) and CEPC (Circular Electron-Positron Collider) outperform the linear collider projects ILC (International Linear Collider) and CLIC (Compact LInear Collider) by orders of magnitude. Above $\sim 500\,\mathrm{GeV}$ linear colliders provide larger luminosities.

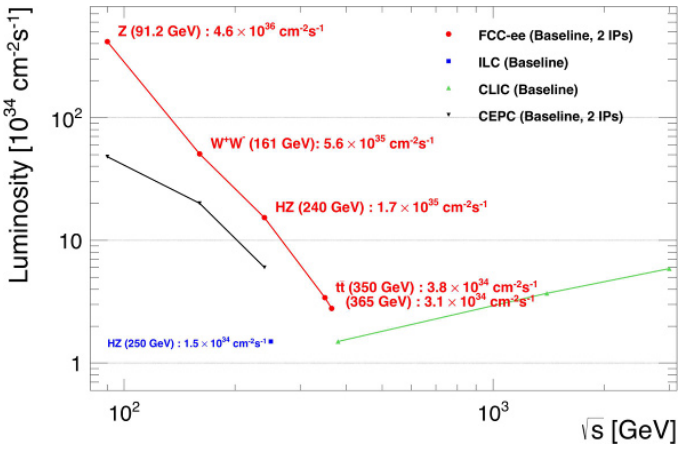

Fig. I.14.3: Expected luminosities for different future collider projects [5]. At energies below $200\,\mathrm{GeV}$ the circular collider projects FCC-ee and CEPC outperform the linear collider projects ILC and CLIC by orders of magnitude. Above $\sim 500\,\mathrm{GeV}$ the linear colliders provide larger luminosities.

Question I.14.4: Why does the luminosity drop for the circular colliders with increasing beam energies? Hint: for FCC-ee the synchrotron radiation power is limited to a maximum of $50\,\mathrm{MW/beam}$ for all operation modes.

I.14.4 Step II: Beam rigidity and required bending fields

Calculate the beam rigidity and the required integrated dipole field in order to determine the magnet technology needed, the dipole length and number and finally the size of the storage ring without straight sections.

This section provides guidelines on designing the layout of the collider. Once the particle type (lepton vs. hadron) is defined and in the case that the decision has been made in favour of a circular collider, the beam rigidity can be calculated. The beam rigidity provides direct information about the required magnet technology (super-/normal-conducting), deflection angle and, eventually, the circumference of the collider ring.

I.14.4.1 What is the general layout of a circular collider?

A circular collider consists of arc sections and straight sections. The straight sections house injection/extraction sections, RF installations, collimation sections, where particles with large amplitude or momentum offset are filtered out safely, special beam diagnostics, and of course the interaction regions with mini-beta insertions.

Besides bending the beam and transporting it to the next straight section, a crucial purpose of the arc sections is to control tune and chromaticity. Sometimes also higher-order multipoles are installed for higher-order optics corrections. The integrated magnetic field in arc sections defines the beam energy. In case of lepton storage rings, lattice and optics of the arc sections define the beam emittance (see Section I.14.5.8). Optics variations in the arc sections allow to tune the beam emittance.

Figure I.14.4 shows the layout of the LHC, which features an eight-fold symmetry and, thus, eight arc and eight straight sections. Often, about two thirds of the circumference consist of arc sections and about one third consists of straight sections.

I.14.4.2 How are beam energy and circumference of the accelerator related?

The deflection angle of charged particles in a magnetic dipole field depends on the particle momentum or, in other words, the beam energy. For higher energies, either the bending radius ρ increases or, for a fixed footprint, the magnetic field B has to be increased.

In the case of a storage ring, a given particle momentum defines the required integrated magnetic field along the design orbit. This can be easily shown considering an infinitesimal arc element

$$\mathrm{d}\theta = \frac{\mathrm{d}s}{\rho} = \frac{B\,\mathrm{d}s}{B\rho} = \frac{e}{p_0} B\,\mathrm{ds}, \tag{I.14.5}$$

where ρ is the bending radius and s denotes the longitudinal coordinate of the Frenet-Serret coordinate system. In the calculation, the relation of the beam rigidity (see Chapter I.3 on transverse beam dynamics) has been used: $B\rho = p_0/e$. Integration of the left side from 0 to 2π yields Eq. (I.14.4), that is here repeated for convenience

$$\oint B\,\mathrm{d}s = 2\pi\frac{p_0}{e}.$$

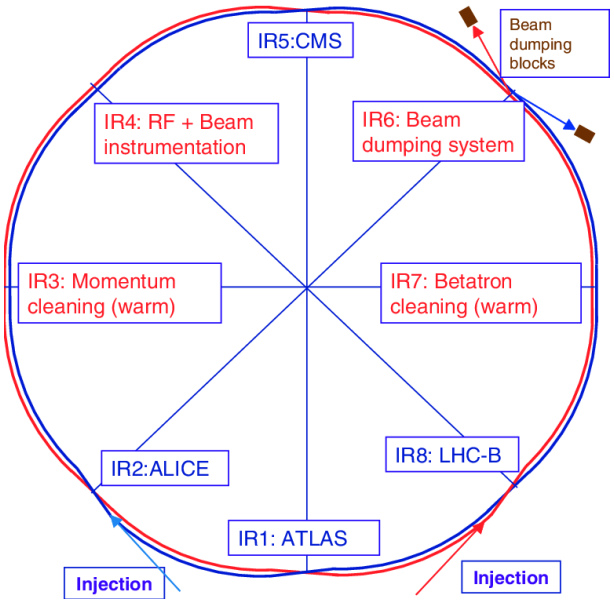

Fig. I.14.4: Layout of the LHC [6]. Two straight sections are taken by the two multi-purpose experiments ATLAS and CMS. The straight sections with the smaller experiments ALICE and LHCb also include the injection sections. In two straight sections, collimators are installed for momentum cleaning and transverse betatron cleaning, one houses the RF section and the last one contains the extraction section towards the beam dump.

The direct consequence: the pursuit of ever higher beam energies in hadron colliders requires to push the magnetic field strengths up to their technical limit. Once the limit is reached, higher energies can only be obtained via a larger circumference of the storage ring, which is why each future high-energy circular collider project increases in circumference. In the end, the beam energy is limited by the maximum tolerable circumference affordable within a given budget.

Question I.14.5: What is the maximum momentum of protons in the LHC? LHC has $N = 1232$ bending magnets each with a length of $L_\mathrm{B} = 14.3\,\mathrm{m}$ and a magnetic field strength of $B = 8.3\,\mathrm{T}$.

I.14.4.3 Shall we use normal- or superconducting magnet technology?

The choice of the magnet technology depends on the beam energy and the particle species.

As we established above, high-energy hadron accelerators are designed as exploratory machines and push on the energy frontier. As the magnetic field of iron dominated magnets is limited to $< 2\,\mathrm{T}$, they require superconducting magnet technology to reach their energy at an acceptable circumference. Using superconducting magnets, the energy loss due to the electric resistance in the magnet coils is reduced drastically at the expense of a cryogenic infrastructure.

In the case of electron-positron storage rings, an additional limitation has to be considered: due to the much smaller mass of electrons and positrons, the emitted synchrotron radiation power proportional to E^4/ρ^2 becomes unbearable – typically long before the technical limit of the magnetic fields is reached. Designers of high-energy lepton colliders still aim for large circumferences with the following strategy in

mind: decreasing the bending fields as well as distributing them over the ring as much as possible results in large bending radii ρ, which in turn reduces the synchrotron radiation power. As a consequence, the required magnetic field strengths can be realised with normal-conducting magnet technology.

As a side note, the final-focusing quadrupoles of the FCC-ee collider will need to be installed inside the detector. In this case, superconducting magnets are being discussed, which then allows for more compact designs in order to reduce the blind spots of the detector. These superconducting elements then need to be protected from synchrotron radiation to prevent quenches.

Question I.14.6: Calculate the bending field of the dipoles of FCC-ee during $t\bar{t}$ production at $182.5\,\mathrm{GeV}$ beam energy assuming a local bending radius of $\rho = 10.760\,\mathrm{km}$. Which magnet technology do you propose based on your result?

I.14.5 Step III: Focusing structure and beam optics

Determine the focusing structure of the basic cell: FODO, DBA, etc. Calculate the optics parameters of the basic cell: beam dimension, vacuum chamber, magnet aperture & design, and tune.

This section discusses various basic cell structures for the lattice design. Depending on the purpose of the accelerator, e.g. a collider or a light source, different lattices can be beneficial. In the particular case of a FODO basic cell, some design considerations are presented as guidelines for various particle species. Additional information is provided in the textbooks [7, 8] or the CAS proceedings [9–11].

I.14.5.1 Why is the FODO cell an adequate basic cell for high-energy storage rings?

As the name says, high-energy storage rings accommodate particle beams of highest possible beam energies, which are then collided to study the fundamental physics of the standard model and beyond. The design of the basic lattice cell is driven by the requirement of a high dipole filling factor, which applies for both hadron and lepton storage rings but for different reasons.

Hadron storage rings: Hadrons, such as protons or heavy ions are used for exploratory machines that push on the energy frontier. The beam energy is defined by the integrated magnetic field, which is pushed towards the technical limit during the design process. For a given magnetic field and circumference the energy can be maximised if the largest possible proportion of the cell is occupied by dipoles.

Lepton storage rings: Contrary to hadrons, the beam dynamics of leptons is dominated by the emission of synchrotron radiation. The synchrotron radiation power P_γ is proportional to E^4/ρ. To reduce it, the local bending radius ρ is maximised, i.e., the local magnetic field strength is minimised. The design strategy is to again maximise the proportion of the cell occupied by dipoles, this time not to maximise the integrated magnetic field but rather to minimise the local magnetic field and, thus, synchrotron radiation power.

The common feature of high-energy hadron and lepton storage rings is that the lattice design of the basic cell should push for a highest possible dipole filling factor, which is the ratio between the length

of all dipole magnets and the cell length. The FODO cell allows for a very large dipole filling factor and is typically chosen as the basic cell of high-energy storage rings.

I.14.5.2 How is a FODO structured?

The FODO structure consists of equidistant quadrupoles with alternating polarity. The space in between the quadrupoles can either consist of drift spaces or can be filled with other equipment such as bending magnets or RF cavities. Compared to other lattice structures it features a low number of quadrupoles. The FODO structure is used in transfer lines which have to cover long distances with a minimum of hardware, in linacs or in FELs (Free Electron Lasers) which require lots of space for RF cavities or undulators, and in circular colliders which require a high dipole filling factor.

Figure I.14.5 shows the lattice of a $50\,\mathrm{m}$ long FODO cell that has been proposed for FCC-ee [12]. The cell starts and ends in the centre of a (horizontally) focusing quadrupole represented by the box above the horizontal line. The defocusing quadrupole is located in the centre depicted by the box below the horizontal line. The small boxes next to the quadrupoles are sextupole magnets, which are installed for chromaticity correction. The dipole filling factor of a FODO cell should reach at least $80\,\%$. The four dipole magnets, represented by the huge boxes, have a length of $10.5\,\mathrm{m}$ each resulting in a dipole filling factor of $84\,\%$. Underneath, the optics functions β_x, β_y and the horizontal dispersion function D_x are plotted. x and y denote the horizontal and the vertical coordinates of the Frenet-Serret coordinate system. Since quadrupoles focus in one plane while defocusing in the perpendicular plane, the β-function reaches its maximum in one plane where it is at a minimum in the other. The dispersion function follows the course of the horizontal β-function.

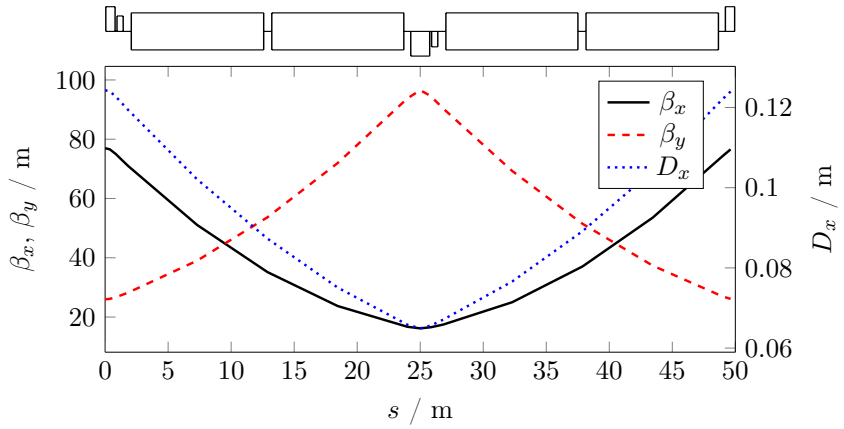

Fig. I.14.5: Lattice and optics functions of a FODO cell that has been proposed for FCC-ee [12]. The large blocks are the dipole magnets and the rectangles above and below the centre line show the position of the quadrupole magnets. The smaller rectangles next to them represent sextupoles.

The simple layout of the FODO cell allows for easy analytical optics calculations. We know from the Chapter I.3 on transverse beam dynamics that the maximum and minimum values of the β-function in a FODO cell of length L_c with phase advance φ are given by

$$\hat{\beta} = L_\mathrm{c}\frac{1+\sin(\varphi/2)}{\sin\varphi} \qquad \text{and} \qquad \check{\beta} = L_\mathrm{c}\frac{1-\sin(\varphi/2)}{\sin\varphi}. \tag{I.14.6}$$

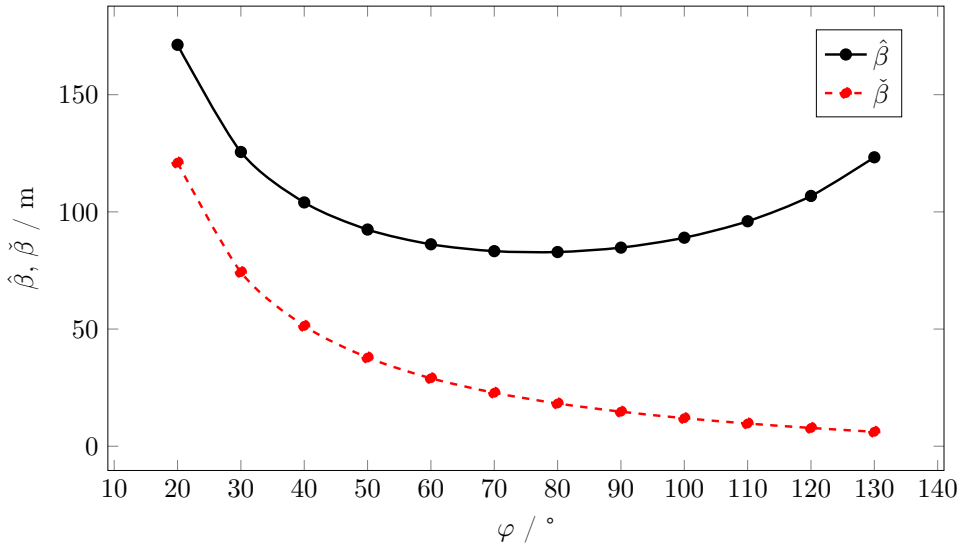

Fig. I.14.6: Minimum and maximum values of the β-function as function of phase advance per cell for the FODO cell of Fig. I.14.5. While the minimum value of the β-function decreases with increasing phase advance, the maximum value has a minimum at $\varphi = 76°$.

The minimum value for $\hat{\beta}$ is obtained for $\varphi = 76°$ as shown in Fig. I.14.6. $\check{\beta}$ continuously decreases with increasing phase advance. This discussion already shows: the most important parameters to be determined during the lattice design are the cell length as well as the phase advance per cell.

I.14.5.3 How do we choose the phase advance of a FODO cell for a hadron storage ring?

The Chapter I.3 on tranverse beam dynamics discusses that, in hadron storage rings, the geometric emittance ϵ shrinks during acceleration because of adiabatic damping

$$\epsilon \propto \frac{1}{\beta\gamma}. \tag{I.14.7}$$

Note that in this case β and γ do not refer to the optics functions but to $\beta = v/c$ and to the Lorentz factor γ. As a consequence, the aperture is constrained most at injection energy, as shown in Fig. I.14.7. The transverse $7\,\sigma$ silhouette of the HERA proton beam at $40\,\mathrm{GeV}$ injection energy ($\gamma = 43$) fills the vacuum chamber almost entirely. After ramping up the beam energy to a flat-top energy of $920\,\mathrm{GeV}$ (corresponding to $\gamma = 980$), the emittance decreased from $\epsilon = 120\,\mathrm{nm}$ to $\epsilon = 5.1\,\mathrm{nm}$.

Long-time experience from HERA, for example, and tracking studies of beam losses have shown that the aperture at injection should be in the order of at least ± 10 times the beam size σ to provide sufficient space for the beam and prevent particle losses. To maximise the range of beam energies, the phase advance is chosen such that one obtains as small β-functions as possible. As hadron storage rings feature round beams in the sense of $\epsilon_y \approx \epsilon_x = \epsilon$, the β-function should be minimised in both planes at the same time

$$r^2 = \epsilon_x\beta_x + \epsilon_y\beta_y \qquad \rightarrow r^2/\epsilon = \beta_x + \beta_y. \tag{I.14.8}$$

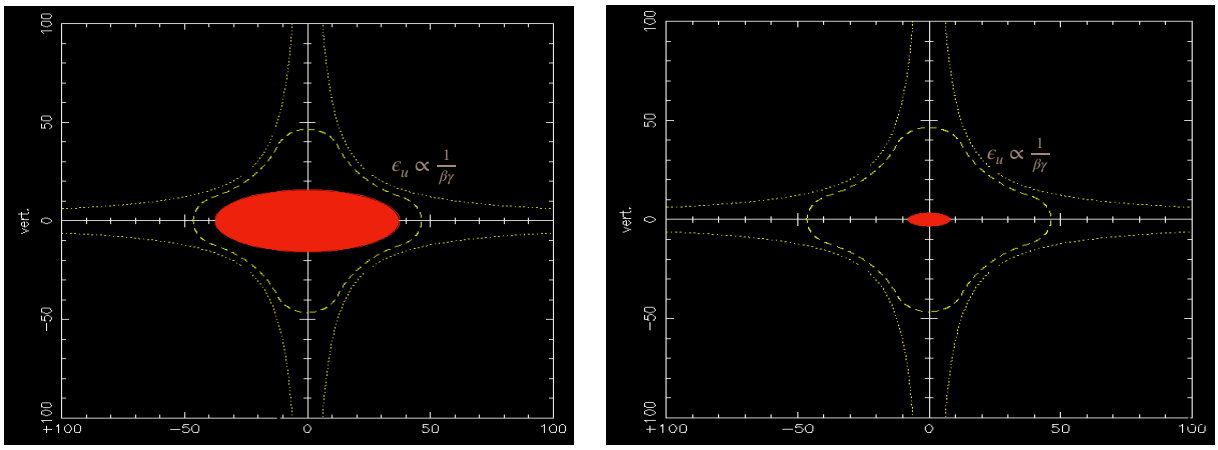

(a) (b)

Fig. I.14.7: Transverse beam cross section ($7\,\sigma$) in the HERA proton ring (a) at injection energy of 40 GeV and (b) at 920 GeV flat-top energy. The beam size shrinks during acceleration due to adiabatic damping.

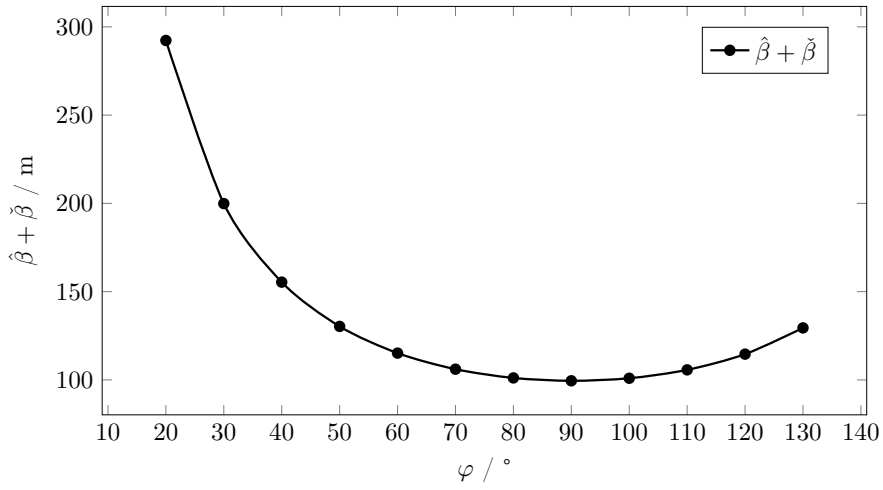

Fig. I.14.8: $\hat{\beta} + \check{\beta}$ as a function of the FODO cell phase advance. The minimum value and thus the minimum sum of transverse beam sizes is obtained for a FODO cell phase advance of $\varphi = 90°$.

The condition for maximum aperture with respect to the beam size,

$$\frac{\mathrm{d}}{\mathrm{d}\varphi}(\hat{\beta} + \check{\beta}) = \frac{\mathrm{d}}{\mathrm{d}\varphi}\frac{2L_\mathrm{c}}{\sin\varphi} = -2L_\mathrm{c}\frac{\cos\varphi}{\sin^2\varphi} \stackrel{!}{=} 0, \tag{I.14.9}$$

is fulfilled for a phase advance of $\varphi = 90°$. Figure I.14.8 illustrates this by plotting the sum of $\hat{\beta}$ and $\check{\beta}$ as a function of the phase advance per cell φ. With $\varphi = 90°$, Eq. (I.14.6) becomes

$$\hat{\beta} = L_\mathrm{c}\left(1 + \frac{1}{\sqrt{2}}\right). \tag{I.14.10}$$

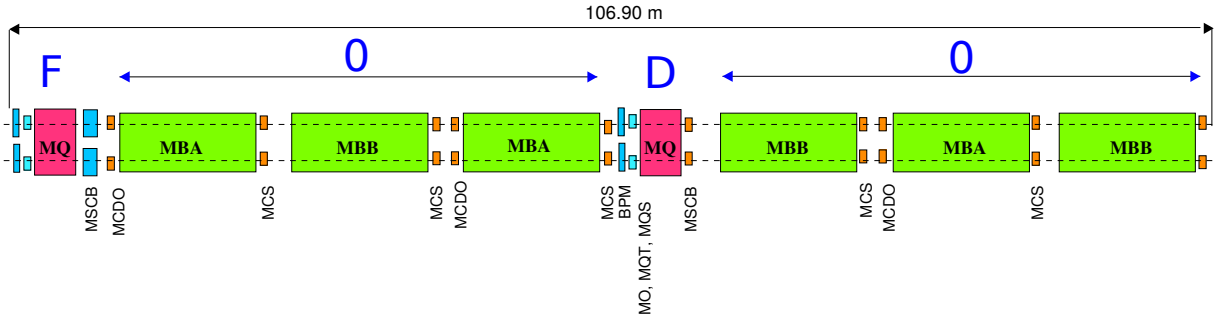

Fig. I.14.9: Layout of an LHC FODO cell including arc corrector magnets according to the design report [13]: in addition to the main quadrupoles (MQ) and bending magnets (MBA/MBB), the correctors comprise trim quadrupoles (MQT), skew trim quadrupoles (MQS), spool piece sextupoles (MCS), lattice octupoles (MO), spool piece octupole and decapole (MCOD), and sextupole (skew sextupole) and orbit corrector (MSCB).

We note that the maximum beta function depends linearly on the cell length L. As a consequence, the transverse rms beam size $\sigma \approx \sqrt{\epsilon\beta}$ is approximately proportional to the square root of the cell length. This gives the possibility to adjust the maximum beam size according to the aperture availability. Besides the beam size at injection energy, the aperture is also constrained by the magnetic field strength

$$B = \frac{\mu_0 n I}{d}, \tag{I.14.11}$$

where I denotes the current in the n windings of the coil, and d is the pole gap (twice the aperture). The larger the pole gap (i.e. the aperture), the smaller the resulting magnetic field becomes. Since the goal is to increase the integrated magnetic field as much as possible, small pole gaps are generally preferred. However, small pole gaps would require small beta functions and thus short cells. Short cells on the other hand provide a smaller dipole filling factor. Clearly, a good balance must be found for all these counteracting aspects in order to determine an optimum cell length, which is an essential task of lattice designers.

Example - the FODO cell of LHC: The schematic layout of an LHC FODO cell is shown in Fig. I.14.9. Here, three bending magnets are installed in between two quadrupoles magnets. The bending magnets are each $14.3\,\mathrm{m}$ long, leading to a dipole filling factor of $80\,\%$. In addition to the main quadrupoles (MQ) and bending magnets (MBA/MBB), a set of corrector magnets is installed to compensate for magnetic higher-order multipole fields, which arise from eddy currents during the energy ramp.

Question I.14.7: The FODO cell of LHC has a length of $L = 106.9\,\mathrm{m}$ and a phase advance of $\varphi = 90°$. Use Eq. (I.14.6) to calculate the values of the maximum and minimum β-function in the LHC FODO cell. The figure below [14] shows the optics functions calculated by MAD-X. Do the values agree?

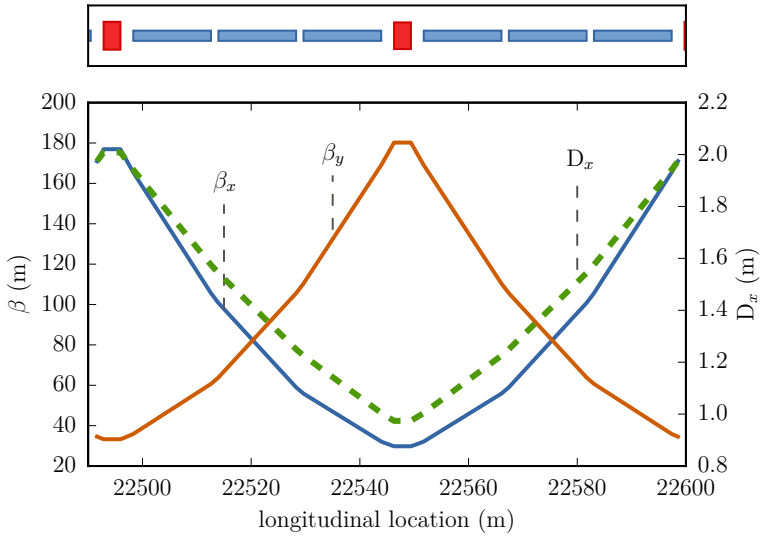

I.14.5.4 Summary: Hadron storage rings

Features of hadron storage rings that have to be taken into account for the lattice design process:

- The beam emittance in a hadron storage ring is typically defined by the beam quality delivered by injectors.
- Hadron storage rings often feature round beams in the sense of $\epsilon_y \approx \epsilon_x$.
- The emittance shrinks during acceleration (adiabatic damping): $\epsilon_x \propto \frac{1}{\beta\gamma}$.
- Aperture requirements call for smallest sum of β-functions and thus for a FODO cell phase advance per cell of $\varphi = 90°$.
  $\rightarrow$ The maximum value of the β-function is then defined via the cell length: $\hat{\beta} = L_c \left(1 + \frac{1}{\sqrt{2}}\right)$.
  $\rightarrow$ The cell length is chosen according to aperture availability in the bending magnets.
- Maximum beam energy is obtained through maximizing the integrated B field: $\int B \, \mathrm{d}s = 2\pi \frac{p_0}{e}$.
  $\rightarrow$ Highest possible dipole fields are required.
  $\rightarrow$ Maximum dipole filling factor is required.

I.14.5.5 What is the fundamental difference between a hadron and lepton storage ring?

The beam dynamics in a lepton storage ring is dominated by the emission of synchrotron radiation, which in the case of hadron storage rings only significantly occurs for beam energies starting from the TeV range. The emission of synchrotron radiation leads to two fundamental effects, namely radiation damping and quantum excitation. These decrease or increase the beam emittance, respectively, until an equilibrium of both effects has been reached after a few damping times. For details to radiation damping and quantum excitation, consult the Chapter I.10 on synchrotron radiation.

For a working point chosen far from linear coupling resonances, the equilibrium beam parameters in a lepton storage ring can be approximately expressed using the following radiation integrals [8]

$$\mathcal{I}_1 = \oint \frac{D_x}{\rho}\,\mathrm{d}s, \tag{I.14.12}$$

$$\mathcal{I}_2 = \oint \frac{1}{\rho^2}\,\mathrm{d}s, \tag{I.14.13}$$

$$\mathcal{I}_3 = \oint \frac{1}{|\rho^3|}\,\mathrm{d}s, \tag{I.14.14}$$

$$\mathcal{I}_4 = \oint \frac{D_x}{\rho}\left(\frac{1}{\rho^2} + 2k_1\right)\mathrm{d}s, \tag{I.14.15}$$

$$\mathcal{I}_5 = \oint \frac{1}{|\rho|^3}\mathcal{H}_x\,\mathrm{d}s, \tag{I.14.16}$$

where k_1 denotes the quadrupole strength, and the $\mathcal{H}_x$ function is given by

$$\mathcal{H}_x = \beta_x D_x'^2 + 2\alpha_x D_x D_x' + \gamma_x D_x^2 \tag{I.14.17}$$

using the optics functions β_x, α_x, and γ_x. The synchrotron radiation integrals mainly depend on the local bending radius ρ and the dispersion function D_x. In other words, the equilibrium beam parameters can be tailored during the lattice design. This is an important insight.

The first synchrotron radiation integral is related to the momentum compaction factor

$$\alpha_\mathrm{c} = \frac{\mathcal{I}_1}{C}, \tag{I.14.18}$$

where C is the machine circumference. The second integral in combination with the third synchrotron radiation integral gives the equilibrium energy spread

$$\frac{\sigma_\mathrm{E}^2}{E^2} = C_\mathrm{q}\gamma^2\frac{\mathcal{I}_3}{J_s\mathcal{I}_2}. \tag{I.14.19}$$

For electrons or positrons the constant $C_\mathrm{q} = \frac{55}{32\sqrt{3}}\frac{\hbar c}{m_0 c^2}$ has the value $3.832 \times 10^{-13}\,\mathrm{m}$. γ in this case is again the Lorentz factor. The damping partition numbers can be expressed using the second and forth integral,

$$J_x = 1 - \frac{\mathcal{I}_4}{\mathcal{I}_2} \quad \text{and} \quad J_s = 2 + \frac{\mathcal{I}_4}{\mathcal{I}_2}, \tag{I.14.20}$$

and finally the equilibrium emittance is defined by the ratio of the fifth and second integral

$$\epsilon_x = C_\mathrm{q}\frac{\gamma^2}{J_x}\frac{\mathcal{I}_5}{\mathcal{I}_2}. \tag{I.14.21}$$

The energy loss per turn due to synchrotron radiation is given by

$$U_0 = \int_0^{T_0} P_\gamma\,\mathrm{d}t = \frac{C_\gamma}{2\pi}E^4\mathcal{I}_2 \tag{I.14.22}$$

with the revolution time T_0 and $C_\gamma = \frac{e^2}{3\epsilon_0}\frac{1}{(m_\mathrm{e}c^2)^4} = 8.8460 \times 10^{-5}\,\mathrm{m\,GeV^{-3}}$. U_0 increases with the

beam energy E to the fourth power. As a consequence, beam energy, beam current, and in the end the luminosity of high-energy lepton storage rings are limited by the maximum acceptable synchrotron radiation power, which both has to be absorbed by collimators and returned to the beam in the RF cavities.

In the example case of FCC-ee, the maximum synchrotron radiation power has been limited to $50\,\mathrm{MW}$ per beam. As mentioned in an earlier section, four operation schemes are foreseen for FCC-ee for precision measurements of the Z, W, and Higgs bosons and the $t\bar{t}$ threshold. Table I.14.1 shows the number of bunches, particles per bunch and luminosity at the corresponding beam energies that range from $45.6\,\mathrm{GeV}$ to $182.5\,\mathrm{GeV}$ as presented in the conceptual design report [5]. In order to keep the power loss constant, the number of bunches naturally decreases with increasing beam energy. The instantaneous luminosity for the corresponding mode correspondingly decreases by two orders of magnitude.

Table I.14.1: Beam energy, number of bunches, number of particles per bunch and luminosity for the four operation modes of FCC-ee as presented in the conceptual design report [5]. Since the synchrotron radiation power is limited to the same value in all modes, luminosity reduces due to the diminishing number of bunches.

Energy (GeV)	# bunches	# particles per bunch (10^{11})	Luminosity ($10^{34}\,\mathrm{cm}^{-2}\,\mathrm{s}^{-1}$)
45.6	16 640	1.7	460.0
80.0	2000	1.5	56.0
120.0	328	1.8	17.0
182.5	48	2.3	3.1

The beam dynamics of electron and positron storage rings is determined by emission of synchrotron radiation. The synchrotron radiation power is determined by the lattice. The lattice design allows to tailor the emission of synchrotron radiation and, thus, beam dynamics and beam parameters.

Let's go step by step...

I.14.5.6 How do we choose the phase advance of a FODO cell for a lepton storage ring?

Quantum excitation, the effect that leads to an increase of the emittance, only occurs in dispersive regions (i.e., where the dispersion function $D \neq 0$). This means, in an ideal ring, where the vertical dispersion function is zero everywhere, only radiation damping occurs and the vertical emittance could become infinitely small in a classical sense. In a real storage ring, the vertical emittance is effectively determined by elements that introduce coupling between the transverse planes, such as sextupoles for example, and finite vertical dispersion which arises from misalignments. In the end, the vertical emittance ϵ_y typically assumes values in the order of $0.1\,\%$ to $1\,\%$ of the horizontal emittance ϵ_x. This is why lepton storage rings typically feature "flat" beams in the sense of $\epsilon_x \gg \epsilon_y$.

In hadron storage rings with "round" beams, the sum of maximum and minimum values of the β-function has been optimised for largest aperture. In the case of lepton storage rings with flat beams,

only $\hat{\beta}$ is considered and minimised

$$\frac{\mathrm{d}}{\mathrm{d}\varphi}\hat{\beta} = \frac{\mathrm{d}}{\mathrm{d}\varphi}\left[\frac{L_\mathrm{c}(1+\sin(\varphi/2))}{\sin(\varphi)}\right] = 0 \quad \rightarrow \varphi = 76^\circ. \tag{I.14.23}$$

The minimum value of the maximum β-function is, hence, obtained for a phase advance per cell of $\varphi = 76^\circ$ in both planes, which can be readily identified in Fig. I.14.6.

Even though minimum beam sizes are obtained for a advance per cell of $\varphi = 76^\circ$, this value is often not chosen because of following reason: we know from the Chapter I.3 on transverse beam dynamics, that an energy offset of a particle creates a focusing error in the quadrupoles, which is captured by the quantity called chromaticity. The chromaticity is compensated by sextupole magnets, which need to be located in dispersive regions. The magnetic field of a sextupole is given by

$$\frac{e}{p}B_x = k_2\, xy \qquad \text{and} \qquad \frac{e}{p}B_y = \frac{1}{2}k_2(x^2 - y^2), \tag{I.14.24}$$

where k_2 is the sextupole strength. The nonlinear nature of the sextupolar field perturbs the harmonic transverse oscillation of the particles by introducing geometric aberrations that arise from particle position and angle. However, such geometric aberrations can be canceled, if two sextupoles with equal length and strength are installed at positions with a relative phase advance of (an odd multiple of) π, which is then called a *-I transformation*. To allow such an arrangement, low multiples of the phase advance per FODO cell should ideally add up to 180°. Typical phase advances in lepton storage rings are:

$$\varphi = 90^\circ \Rightarrow 2 \times \varphi = \pi,$$
$$\varphi = 60^\circ \Rightarrow 3 \times \varphi = \pi.$$

I.14.5.6.1 Cancellation of geometric aberrations of sextupoles using a "-I transformation"

To counteract the influence of geometric aberrations, which is particularly notable for particles at large betatron oscillation amplitudes, the lattice should comprise as many sextupoles as possible. This measure allows to minimise the strength of localised nonlinear fields. Should the stability of the particle motion still be compromised at reasonably small betatron amplitude due to geometric aberrations, a more elaborate sextupole scheme becomes necessary: the geometric effects of the sextupoles can be canceled by installing them in pairs with equal strength, and ensuring that the separating transfer matrix for x, x', y, and y' constitutes a negative unity transformation

$$-I = \begin{pmatrix} -1 & 0 & 0 & 0 \\ 0 & -1 & 0 & 0 \\ 0 & 0 & -1 & 0 \\ 0 & 0 & 0 & -1 \end{pmatrix}. \tag{I.14.25}$$

The contribution of the sextupoles to the overall chromaticity oscillates with the beta function and, thus, at twice the phase advance. This allows to effectively cancel the geometric aberrations imposed by the sextupolar nonlinearity (theoretically at all amplitudes when considering thin lenses) while fully providing for chromaticity correction with each sextupole.

Question I.14.8: Show the cancellation of nonlinear sextupole contributions for the two sextupoles S1 and S2, which are separated by a $-I$ transformation as illustrated in the schematic below [12].

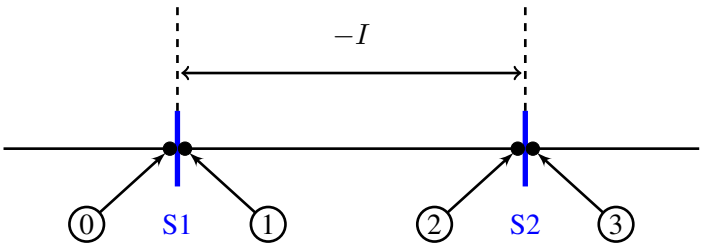

The particle arrives at point 0 in front of sextupole S1 with coordinates (x_0,y_0) at an angle specified by (x_0',y_0'). In thin-lens approximation, sextupoles generate single kicks:

$$\Delta x' = \frac{1}{2}\,(k_2 L_\mathrm{S})\,(x^2 - y^2), \tag{I.14.26}$$

$$\Delta y' = (k_2 L_\mathrm{S})\,x\,y. \tag{I.14.27}$$

Calculate particle the coordinates and angle at point 3 just behind S2.

Consequently, an effective chromaticity correction scheme necessitates an even number of sextupoles, while efforts should be made to minimise phase advance errors as they diminish the efficiency of cancellation [15]. In a strict sense, the compensation of geometric effects as described above only holds true for thin lenses. The finite length of sextupoles introduces higher-order terms [16], which cannot be fully eliminated by the $-I$ transfer map. Nevertheless, while the full cancellation of first-order geometric aberrations may not be achieved, they can still be significantly reduced.

I.14.5.7 What are possible sextupole schemes for high-energy storage rings?

Sextupoles are categorised into focusing and defocusing sextupoles correcting chromaticity in the horizontal and vertical plane, respectively. A sextupole family refers to a group of sextupoles with the same strength. Taking above mentioned considerations into account, the sextupoles of a family should be installed with a phase advance separation of π. The number of families is determined by the phase advance per cell.

For a phase advance of 60°, three families can be installed for each plane: the sextupole in the first cell belongs to the first family, the one in the second cell to the second family, and the one in the third cell to the third family. The sextupole in the fourth cell is installed with a phase advance of π relative to the first sextupole, so it needs to have the same strength as the first one to cancel its geometric aberrations and thus belongs to the first family. Other phase advances per cell and their corresponding number of sextupole families are listed in Tab. I.14.2.

The arrangement of sextupoles into families is a critical aspect for the design of a chromaticity compensation scheme and should be done carefully. The number of families determines the degrees of freedom for chromaticity correction and depends on lattice and optics. There are two primary methods

Table I.14.2: Possible FODO cell phase advances to establish a multi-family sextupole scheme in the arc sections and the corresponding number of sextupole families.

Phase advance		# of families
$\pi/4$	$45°$	4
$\pi/3$	$60°$	3
$\pi/2$	$90°$	2
$3\pi/5$	$108°$	5
$3\pi/4$	$135°$	4

for organizing sextupole within the lattice: interleaved schemes and non-interleaved schemes. Each approach presents its own set of advantages and disadvantages, which will be the subjects in the subsequent discussion.

I.14.5.7.1 Interleaved sextupole scheme

In an interleaved sextupole scheme, sextupoles are installed at every quadrupoles. As the phase advance per cell is smaller than π, this leads to the arrangement discussed above, where the members of the sextupole families are interleaved. Figure I.14.10 illustrates the layout of an interleaved sextupole scheme for a FODO cell lattice with $\varphi = 60°$ and three sextupole families in both planes. The grid represents the FODO cells, the long vertical lines stand for the focusing quadrupoles and the short lines for the defocusing quadrupoles. The sextupoles are installed next to every quadrupole. The first sextupole of each group belongs to the first family "SF1", the second to the second family "SF2", etc.

The main advantage of this arrangement is the high number of sextupoles, which allows to decrease the individual sextupole strengths. This diminishes the local strength of the nonlinear fields, however, the cancellation of geometric aberration is compromised since other sextupoles are installed between two members of a family and the $-I$ transformation is not exactly given.

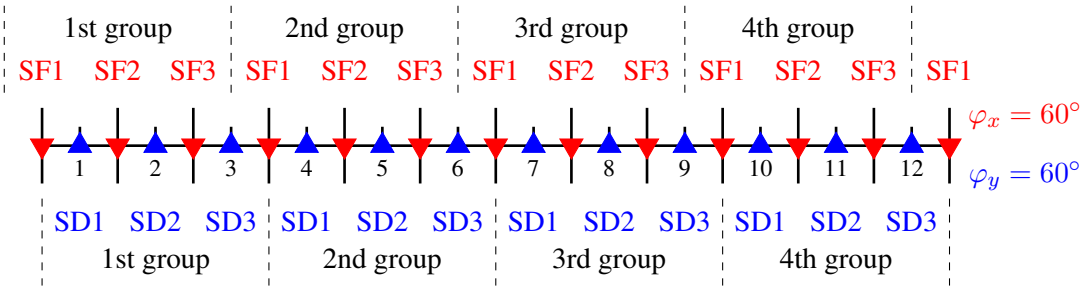

Fig. I.14.10: Interleaved sextupole scheme for a FODO cell phase advance of $\varphi = 60°$ with three families in both planes.

I.14.5.7.2 Non-interleaved sextupole scheme

For the best cancellation of geometric effects the sextupoles should be installed in individual pairs with same strength separated by a $-I$ transfer map. In the ideal case, only linear elements are installed between the two sextupoles. Such a scheme, as illustrated in Fig. I.14.11 for a FODO cell phase advance

$\varphi = 60°$, is called a non-interleaved sextupole scheme. The scheme starts with a pair of focusing sextupoles located at the focusing quadrupoles of the cells 1 and 4. As the phase advance is $60°$, two sextupoles forming a pair are separated by three FODO cells. Since the sextupole pairs shall be not interleaved, the first defocusing sextupole pair is installed next to the defocusing quadrupoles of the cells 4 and 7. A non-interleaved sextupole scheme with non-interleaved sextupole pairs requires many FODO cells. Keeping in mind, that a FODO cell has a length in the order of $100\,\mathrm{m}$, such a scheme is therefore only applicable in large storage rings with long arc sections.

The comparison of Fig. I.14.11 to Fig. I.14.10 directly shows the disadvantage of a non-interleaved sextupole scheme: only 7 sextupoles are installed in the 12 illustrated FODO cells, while 24 are installed in the interleaved scheme. The sextupoles have to correct the same value of the chromaticity and therefore need to be stronger in the non-interleaved scheme.

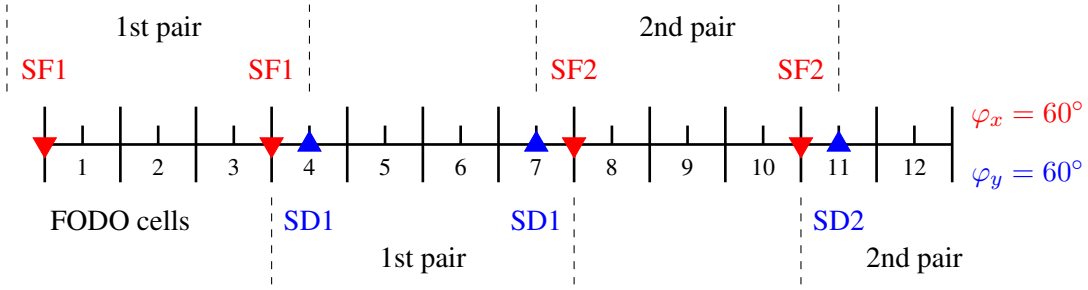

Fig. I.14.11: Completely non-interleaved sextupole scheme for a FODO cell lattice with $\varphi = 60°$ phase advance in both planes. Only linear elements are installed between two sextupoles forming a pair.

I.14.5.7.3 Hybrid schemes

In order to increase the number of sextupoles, many studied and applied non-interleaved schemes interlace the sextupole pairs of the horizontal plane and the vertical plane, but not the sextupole pairs within the same plane. If the difference of the β-functions is large enough, the effect of the sextupoles on the other plane is small and the resulting distortion can be tolerable. The performance of a sextupole scheme in terms of dynamic aperture and momentum acceptance has to be investigated with tracking simulations during the lattice design process of a new accelerator.

I.14.5.7.4 Summary: Sextupole schemes

Interleaved sextupole schemes:

\+ High number of sextupoles and lower local sextupole strength

– Phase relation between two sextupoles of one family is disturbed by interleaved sextupoles

Non-interleaved sextupole schemes:

\+ Better cancellation of geometric aberrations

– Only applicable for many FODO cells

– Stronger sextupoles required

I.14.5.8 With a given phase advance per cell, how can I tune the horizontal emittance?

The natural emittance in an electron storage ring is determined by the equilibrium of quantum excitation, characterised by synchrotron radiation integral $\mathcal{I}_5$, and radiation damping, characterised by synchrotron radiation integral $\mathcal{I}_2$. As mentioned earlier, the two synchrotron radiation integrals are primarily influenced by the bending radius ρ and the dispersion function $D_x(s)$. For a given beam energy, these parameters are thus key factors for adjusting the equilibrium emittance. It has been shown in the Chapter I.3 on transverse beam dynamics that the maximum and minimum value of the dispersion function in a FODO cell can be calculated with the equations

$$\hat{D}_x = \frac{L_\mathrm{c}^2}{\rho}\frac{\left[1+\frac{1}{2}\sin(\varphi/2)\right]}{4\sin^2(\varphi/2)} \qquad \text{and} \qquad \check{D}_x = \frac{L_\mathrm{c}^2}{\rho}\frac{\left[1-\frac{1}{2}\sin(\varphi/2)\right]}{4\sin^2(\varphi/2)}. \tag{I.14.28}$$

The dispersion function and, thus, the equilibrium emittance can be tuned via the cell length, bending radius and phase advance. The plots of these functions in Fig. I.14.12 illustrate that as the phase advance per cell increases, both the maximum and minimum values decrease.

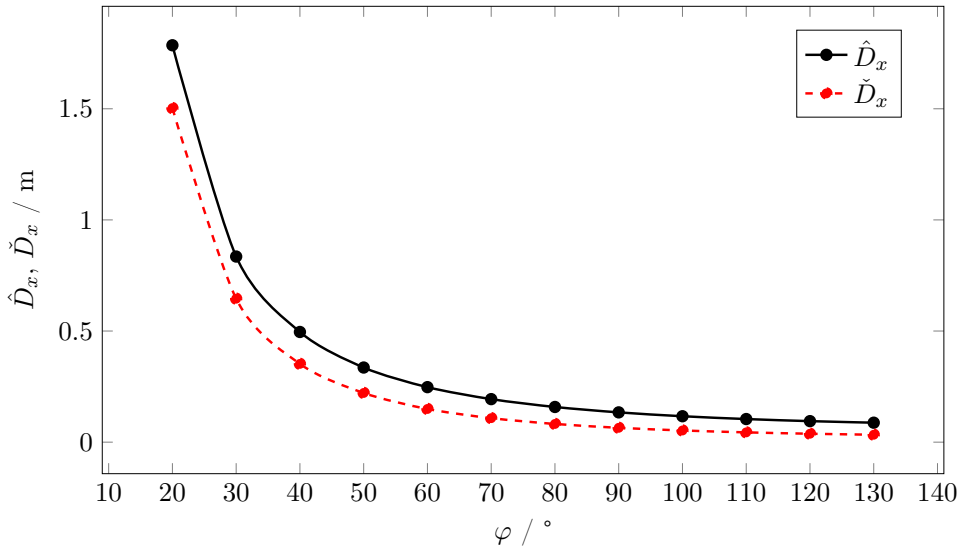

Fig. I.14.12: Minimum and maximum values of dispersion in a FODO cell that has been proposed for FCC-ee as a function of the phase advance per cell.

I.14.5.8.1 Emittance tuning and FODO cell design à la Teng

On the way to low emittance lattices with high brilliance, L.C. Teng presented form factors to calculate the equilibrium emittance in electron storage rings in [17]. In this publication, FODO cells were treated as a "bad example" in terms of low emittance, still, the formalism is useful for the design of a FODO cell delivering a certain value of the equilibrium emittance. In the above mentioned paper, the emittance was written as

$$\epsilon_x = \frac{C_\mathrm{q}}{J_x}\gamma^2\theta^3\, F \qquad \text{with} \qquad F = \frac{\rho^2}{L_\mathrm{B}}\left\langle \mathcal{H}\right\rangle_\mathrm{dipole}. \tag{I.14.29}$$

The quantity θ in this specific case refers to the bending angle of a half-cell with length L. If more than one dipole magnets are installed in a half-cell, θ is the sum of the bending angles of those bending magnets. The same applies for L_B, which is the length of all bending magnets in one half-cell. The bending radius of the dipoles ρ is assumed to be the same for all bending magnets. After some calculations, the form factor for the FODO cell can be expressed as

$$F_\mathrm{FODO} = \frac{1}{2\sin\varphi}\frac{5+3\cos\varphi}{1-\cos\varphi}\frac{L}{L_\mathrm{B}}. \tag{I.14.30}$$

For $\varphi = 90°$ and $\varphi = 60°$ F is then

$$F(90°) = 2.50\frac{L}{L_\mathrm{B}} \qquad \text{and} \qquad F(60°) = 7.51\frac{L}{L_\mathrm{B}}. \tag{I.14.31}$$

Equation (I.14.29) in combination with the form factors of Eqs. (I.14.30) and (I.14.31) can be used for quick analytical estimations during the lattice design phase. Once the beam energy is defined and the dipole filling factor L_B/L has been obtained from a first layout of the FODO cell, a condition for the bending angle θ can be derived to obtain a certain required value of the beam emittance, in this example for a phase advance of $90°$

$$\theta^3 = \frac{1}{2.50}\frac{\epsilon_x J_x}{C_\mathrm{q}\gamma^2}\frac{L_\mathrm{B}}{L}. \tag{I.14.32}$$

The bending angle of a full cell is 2θ, and the number of cells required to close the ring becomes

$$N_\mathrm{c} = \frac{2\pi}{2\theta}. \tag{I.14.33}$$

The circumference of the storage ring without straight sections is then $C = N_\mathrm{c}\, L_\mathrm{c}$. If the obtained circumference is larger than a given limit, the cell length can be scaled down. It is important to keep the dipole filling factor and the bending angle constant, which means that the length of the dipoles must also be scaled and their magnetic field increased. Otherwise the value of the emittance will change.

Side note: increasing the magnetic fields also increases the synchrotron radiation power. If the circumference is below the limit, the cell length can also be scaled up, which decreases the bending magnetic fields and, thus, reduces the synchrotron radiation power.

Question I.14.9: Assume a reasonable dipole filling factor and $J_x = 1$. Calculate the bending angle required to obtain an equilibrium emittance of $\epsilon_x = 1\,\mathrm{nm}$ for an electron beam with the energy of $182.5\,\mathrm{GeV}$. How many cells do you need to close the ring? Is this realistic assuming a cell length of $50\,\mathrm{m}$?

I.14.5.9 Summary: Comparison between circular e^+ e^- colliders and synchrotron light sources

Colliders:

- High beam energy and beam currents lead to tremendous emission of synchrotron radiation.
- FODO structure is used because a high dipole filling factor is required to curb the synchrotron radiation power.
- Large circumference reduces the local bending radius and decreases synchrotron radiation power.
- The emittance is naturally small due to the large circumference.
- Accelerator performance is measured by the luminosity (see Sec. I.14.10.1)

$$\mathcal{L} = \frac{N_1 N_2 n_\mathrm{b} f}{4\pi \sigma_x^* \sigma_y^*}.$$

Synchrotron light sources

- Small footprint is desired.
- Accelerator performance is measured by brilliance of electron beams (see Chapter I.10 on synchrotron radiation)

$$B(\lambda) = \frac{F(\lambda)}{(2\pi)^2 \sigma_x \sigma_{x'} \sigma_y \sigma_{y'}} \propto \frac{1}{\epsilon_x \epsilon_y}$$

  with photon flux $F(\lambda)$.
- Low emittance beams are needed for high brilliance.
- Special low emittance lattices are used to achieve low emittance with small facility footprint.

I.14.5.10 How does a typical low-emittance lattice for synchrotron light sources look like?

To reduce the equilibrium beam emittance the fifth synchrotron radiation integral needs to be as small as possible. Recalling Eqs. (I.14.16) and (I.14.17), the goal is to minimise the dispersion function in places where the beam is deflected, which is unfortunately the place where the dispersion is created. FODO cells are obviously not adequate, because of their high dipole filling factor and large dispersion function. Typical lattice structures designed for low emittances are called *achromat structures*. Achromatic refers to the transverse particle position at the beginning and at the end of the cell, which should be independent of its energy or, in other words, the dispersion function and its derivative vanish.

The prototype of all achromatic lattices is the double bend achromat (DBA) also known as the Chasman–Green-Lattice [18]. The simplest configuration consists of two bending magnets and five quadrupoles: one quadrupole between the two bending magnets and two quadrupoles each in front of the first and behind the second bending magnet. Lattice and optics functions of such an exemplary DBA cell are shown in Fig. I.14.13. Dispersion, vanishing at the start, is created in the first bending magnet. The center quadrupole is horizontally focusing and flips the sign of the derivative. Its strength is adjusted such that the second bending magnet brings the dispersion back to zero. As a consequence of the achromatic optics, no dispersion suppressors are needed and the drift space in-between cells can be increased to

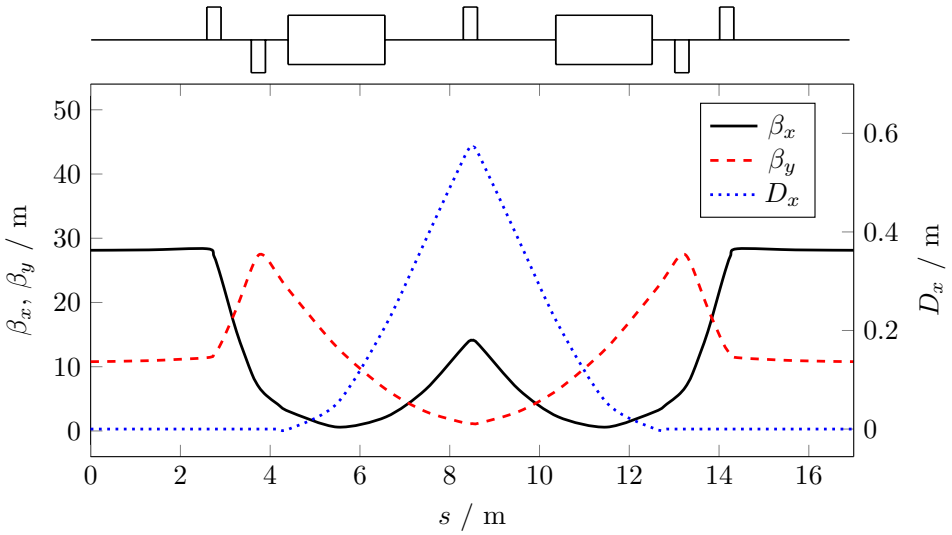

Fig. I.14.13: Lattice and optics of an exemplary Double Bend Achromat cell. Dispersion is created by the first bending magnet and vanishes again after the second one. Flat β-functions in the straight sections enable constant beam sizes within insertion devices.

make space for insertion devices such as wigglers or undulators for dedicated generation of synchrotron radiation. As illustrated in Fig. I.14.13, the optics is matched such that the values of α_x and α_y are small in the drift spaces and the beam size is nearly constant within the insertion devices.

Low emittance at compact footprints in combination with sufficient space for the installation of insertion devices made DBA structures to the characteristic lattice of 3rd generation synchrotron light sources. Such storage rings usually feature the following characteristics:

- Small emittance: $\leq 10\,\mathrm{nm}$,
- Moderate energy spread: $\leq 10^{-3}$,
- Long straight sections for insertion devices: $\sim 5\,\mathrm{m}$,
- High beam current: $> 100\,\mathrm{mA}$.

Question I.14.10: To mitigate certain beam instabilities, optics with negative momentum compaction factor are being discussed. How would one obtain such an optics with a DBA lattice? Remember: the momentum compaction factor is given by $\alpha_\mathrm{c} = \frac{\mathcal{I}_1}{C} = \frac{1}{C} \oint \frac{D(s)}{\rho}\,\mathrm{d}s$.

I.14.5.11 What is the emittance of a DBA structure?

The minimum equilibrium emittance in a DBA lattice is

$$\epsilon_\mathrm{DBA} = \frac{C_\mathrm{q}}{4\sqrt{15}} \gamma^2 \theta^3. \tag{I.14.34}$$

For a detailed derivation we refer to Ref. [11]. Compared to the emittance of a FODO lattice, $\epsilon_\mathrm{FODO} > C_\mathrm{q}\,\gamma^2\,\theta^3$, the emittance of a DBA structure is smaller by a factor of $4\sqrt{15} \approx 15.5$. While

this is already a significant improvement compared to the FODO lattice, the emittance can be reduced even further. Besides the obvious measures of increasing bending angle (circumference) and considering lower beam energy, the contribution to $\mathcal{I}_5$ can be decreased by detuning the quadrupoles and allowing dispersion to leak into the former dispersion-free regions. This allows to decrease the peak dispersion in the centre quadrupole and thus the dispersion in the bending magnets. However, if dispersion leaks into the straight sections where insertion devices are installed, they also contribute to $\mathcal{I}_5$. The dispersion in the insertion devices has to be carefully controlled, to reduce the overall emittance below the value of the ideal DBA structure. At KARA (KArlsruhe Research Accelerator), for example, the emittance has a value of $\epsilon_x = 80\,\mathrm{nm}$ with DBA optics and can be reduced to $60\,\mathrm{nm}$ or even $40\,\mathrm{nm}$ depending on the optics.

I.14.5.12 What is an MBA lattice, and what other lattice design measures are taken in state-of-the-art synchrotron light sources?

The acronym MBA refers to multi-bend achromat. To reduce the emittance even further compared to the DBA lattice, the approach is to split the bending magnets to increase their number while reducing their length. In between two bending magnets, β-functions and dispersion are refocused by quadrupoles. This prevents the dispersion from growing and the contribution to $\mathcal{I}_5$ is diminished. The emittance asymptotically scales with

$$\epsilon \propto \frac{E^2}{N^3}, \tag{I.14.35}$$

where N is the number of bending magnets per cell [19].

The first further development of the DBA lattice was the triple-bend achromat (TBA) lattice with, as the name says, three bending magnets per cell. BESSY II in Berlin comprises a TBA lattice: with a beam energy of $1.7\,\mathrm{GeV}$ and a circumference of $240\,\mathrm{m}$, the equilibrium emittance is about $5\,\mathrm{nm}$, roughly a third of the value that would have been obtained by a DBA lattice.

Modern synchrotron light sources employ achromat cells with six or seven bending magnets are used, the multi-bend achromat cells. They are designed to reach the diffraction limit (see Chapter I.10 on synchrotron radiation), which means the emittance of the electron beam is smaller than the one of the photon beam. Figure I.14.14 shows the optics functions of the unit cell of ESRF-EBS (2015), which has a 7-bend achromat lattice. Compared to the DBA optics of Fig. I.14.13, the values of the dispersion function are reduced by one order of magnitude. While keeping the same circumference and beam energy, the emittance could be reduced from $\epsilon_x = 3.8\,\mathrm{nm}$ to $0.133\,\mathrm{nm}$.

Modern synchrotron light sources are designed to operate 24/7. Because of full-energy injectors and top-up injection it is not necessary anymore to ramp the beam energy. As the main storage ring is designed for one specific beam energy, energy-efficient magnet designs using permanent magnets can be applied. A closer look at the bending magnets in Fig. I.14.14 reveals that the outer bending magnets actually consist of five slices. This is no simulation artefact but rather part of the design: a drawing of this bending magnet is shown in Fig. I.14.15a. The magnet consists of five sections with magnetic fields ranging from $0.17\,\mathrm{T}$ to $0.67\,\mathrm{T}$. The approach to minimise the emittance via $\mathcal{I}_5$ here is to introduce bending magnets with a non-constant magnetic field along their length, they comprise several sections of different field strengths. While keeping the total bending angle constant, the idea of such "longitudinal

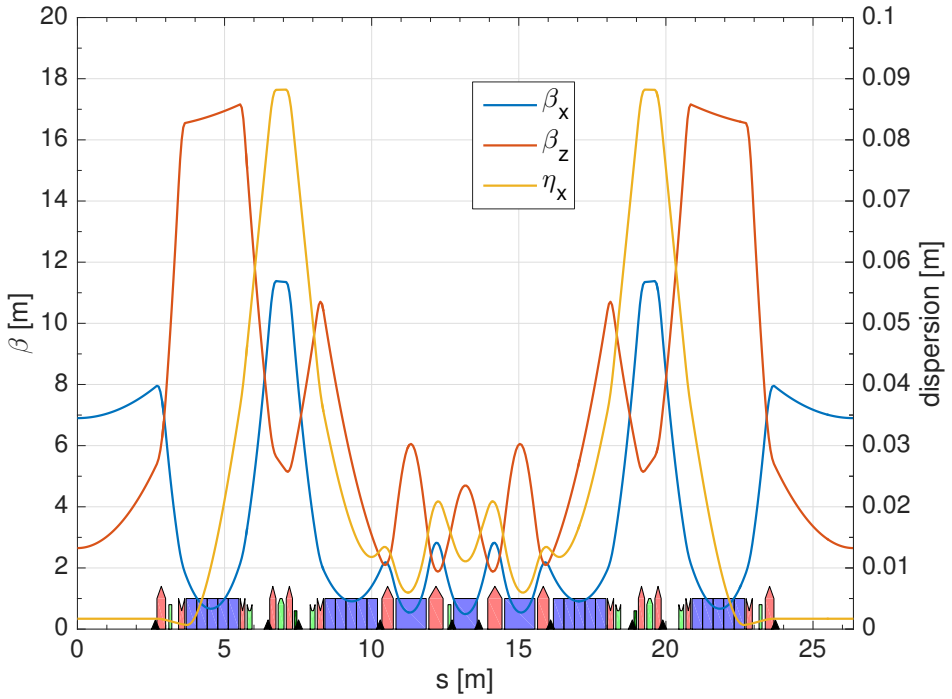

Fig. I.14.14: Seven-bend-achromat optics of ESRF-EBS as presented in 2015 [20]. η_x is the dispersion function, which is usually referred to as D_x in this chapter.

gradient bends" is to have the strongest dipole field where the dispersion is minimum and smaller fields where the larger dispersion would lead to a greater contribution to $\mathcal{I}_5$. The concept is illustrated in Fig. I.14.15b. An added advantage of these longitudinal gradient bends is the ability to produce hard X-rays where the magnetic field is large. More concepts of MBA lattices are discussed in detail in the Chapter I.10 on synchrotron radiation.

Table I.14.3 compares the equilibrium emittances of different electron storage rings with different lattices, circumference and beam energies.

Table I.14.3: Comparison of equilibrium emittance values of different electron storage rings and their lattice type, circumference and beam energy [5, 21–25]. The range at MAX-IV refers to different gap settings of the insertion devices, at KARA for different optics settings.

	lattice	C in m	E in GeV	ϵ_x in nm
LEP II	FODO	26 700	104.0	22.0
FCC-ee	FODO	97 756	182.5	1.46
KARA (DBA optics)	DBA	110	2.5	∼80
KARA (user optics)	DBA	110	2.5	40 to 60
ESRF	DBA	844	6.0	4.0
BESSY II	TBA	240	1.7	5.0
Sirius	6BA	518	3.0	0.251
ESRF-EBS	7BA	844	6.0	0.133
MAX-IV	7BA	528	3.0	0.200 to 0.330

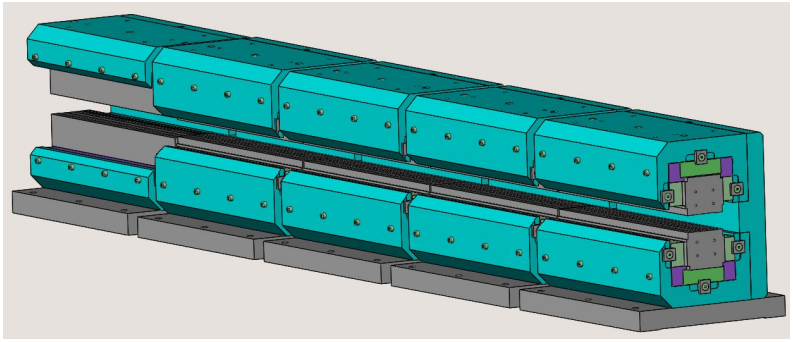

(a)

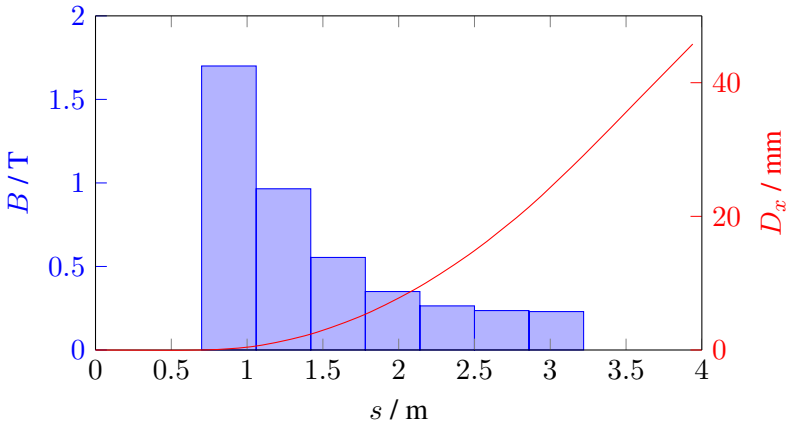

(b)

Fig. I.14.15: (a) Drawing of a longitudinal gradient bend for ESRF-EBS with five sections of different magnetic field ranging from 0.17 T to 0.67 T [20]. (b) Illustration of the longitudinal gradient bend concept (inspired by [20]): the longitudinal gradient bend has high dipole strength where the dispersion is minimum and low fields where the dispersion is large.

I.14.5.13 Summary: Electron storage rings

- Equilibrium of quantum excitation and radiation damping leads to equilibrium beam parameters.
- Equilibrium beam emittance increases with beam energy squared:

$$\epsilon_x = \frac{C_\mathrm{q}}{J_x}\gamma^2\frac{\mathcal{I}_5}{\mathcal{I}_2}.$$

- Electron beams are flat in the sense of $\epsilon_y = 0.1\,\%$ to $1\,\%\epsilon_x$.
- The lattice design allows to tailor the equilibrium beam parameters.
- High energy storage rings: use large bending radius ρ (large circumference) and FODO structure with high dipole filling factor to reduce synchrotron radiation.
- Synchrotron light sources: smaller footprint and room for insertion devices require achromat structures for (ultra-)low emittance.

I.14.6 Step IV: Synchrotron radiation losses and RF sections

Calculate the energy loss per turn: electrons radiate, protons only at energies in the TeV range. Determine the parameters of the RF system: frequency, overall voltage, space needed in the lattice, distribution of RF sections.

This section presents aspects of the lattice design that are related to the energy loss due to synchrotron radiation and the recovery of the lost energy. For a detailed discussion of synchrotron radiation see the corresponding Chapter I.10. For details about cavities and RF systems see the Chapter II.2 on RF engineering and the Chapter II.5 on superconducting RF cavities.

I.14.6.1 What effect does the energy loss due to synchrotron radiation have on the orbit?

The continuous emission of synchrotron radiation in the bending magnets has a strong effect on the closed orbit. Take, for example, a look at Fig. I.14.16, which exhibits the measured beam orbit in LEP: the plot has to be read from the right to the left (direction of motion of the beam) and shows the offset of the beam relative to the design orbit for each beam position monitor along the lattice. The transverse position of the particle is given by the sum of the amplitude of the betatron oscillation x_β and the dispersive offset x_δ (see Section I.14.7.1)

$$x(s) = x_\beta + \underbrace{D_x \delta}_{x_\delta} . \tag{I.14.36}$$

The particles of each beam, both electrons and positrons, lose energy because of the emission of synchrotron radiation. Therefore, the relative energy offset δ increases and the orbit moves toward the inside of the ring in the dispersive arc sections. In the RF sections, the energy of the beam is restored such that the beam is pushed to the outside at the beginning of the next dispersive section reaching nominal energy and design orbit in the centre of the arc. As LEP had four RF sections, this *sawtooth orbit* seen in Fig. I.14.16 features a four-fold symmetry.

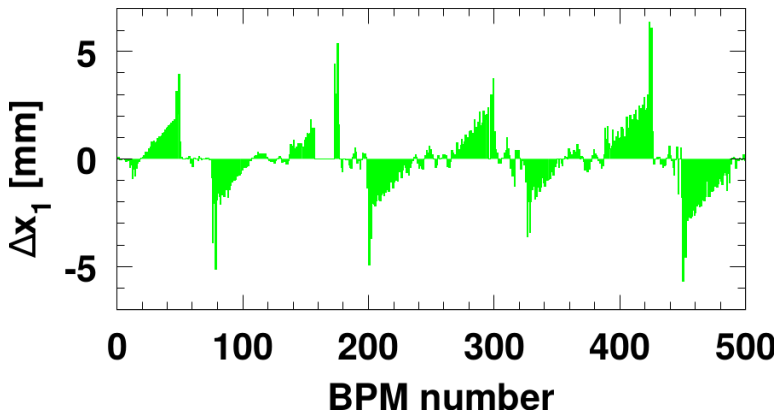

Fig. I.14.16: The orbit offsets in LEP measured at each beam position monitor show the well-known sawtooth shape resulting from the energy loss due to synchrotron radiation and the energy gain in the RF cavities [26]. The direction of motion of the beam is from right to left.

The discussion above shows two things:

1. Should the beam energy not be restored in the RF cavities, the particles will drift to the inside of the ring and eventually hit the vacuum chamber, where they will be lost;
2. The more RF sections are distributed along the ring, the smaller the maximum orbit excursions become. This is of particular importance for high-energy storage rings with high beam energies and huge synchrotron radiation power such as LEP. If the number of RF sections is restricted, modern high-energy lepton storage rings like FCC-ee foresee decreasing magnetic fields along the arc sections that prevent the orbit from drifting. Such an adjustment of the local magnetic field to the local beam energy is referred to as *magnet tapering*.

I.14.6.2 Can we estimate the energy loss per turn from our basic cell?

The energy loss per turn can be calculated with Eq. (I.14.22) and is proportional to $E^4\mathcal{I}_2$. Assuming the total number of dipoles in the ring is N_B and only a single type is used with constant magnetic field without fringe fields, the second synchrotron radiation integral becomes

$$\mathcal{I}_2 = \oint \frac{1}{\rho^2}\mathrm{d}s = \frac{N_\mathrm{B}L_\mathrm{B}}{\rho^2}. \tag{I.14.37}$$

In particular for storage rings with large bending radii ρ, this allows a first analytic estimation of the energy loss per turn as long as beam energy and particle type are well defined.

According to Eq. (I.14.22) the energy loss per turn increases with the fourth power of the beam energy. At the same time C_γ contains the reciprocal mass of the emitting particle. As a consequence, large particle masses suppress the emission of synchrotron radiation. Table I.14.4 summarises the energy loss per turn in storage rings with different particle types and beam energies.

Table I.14.4: Energy loss per turn U_0 in storage rings with different particle species and beam energies E.

	particle	E (GeV)	U_0 (MeV)
LHC	p	7000.0	0.01
FCC-hh	p	100 000.0	5.00
KARA	e^-	2.5	0.63
LEP	e^-	100.0	2850.00
FCC-ee	e^-	182.5	9000.00

I.14.6.3 How can we restore the beam energy?

The Lorentz force for charged particles,

$$\vec{F}_\mathrm{L} = q(\vec{E} + \vec{v} \times \vec{B}), \tag{I.14.38}$$

shows that magnetic fields only act in a direction perpendicular to the particle velocity vector. As a consequence, only electric fields can be used to increase the particle energy. The beam energy is increased

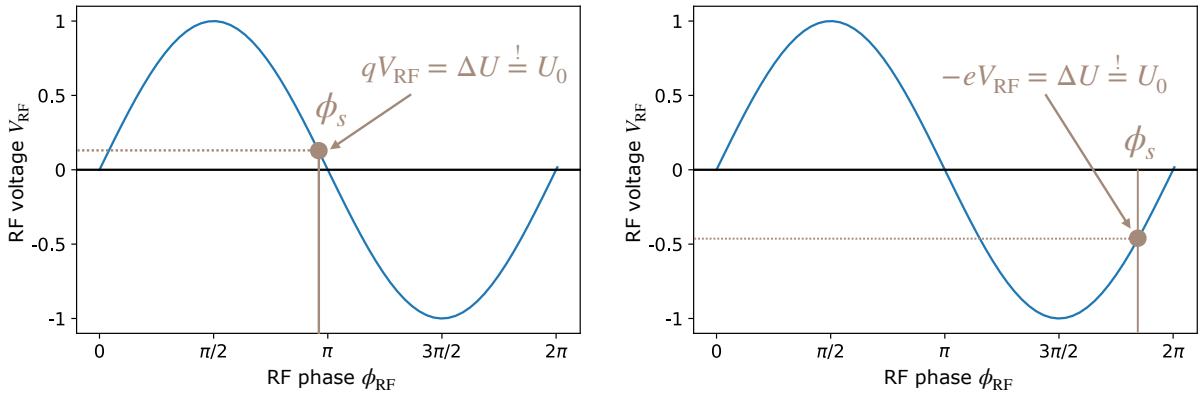

(a) hadrons **(b)** electrons

Fig. I.14.17: The synchronous phase ϕ_s is the RF phase at which the energy gain $\Delta U = qV_{RF}$ equals the energy loss per turn U_0. (a) shows the case for positively charged hadrons, (b) for electrons.

or restored in special sections where RF cavities are installed. They contain the oscillating electric fields in the accelerator.

The energy gain in the cavities ΔU depends on the voltage $V_{RF} = V_0 \sin(\phi_{RF} - \omega_{RF} t)$ in the RF cavity and the phase ϕ_{RF} at the time when the particle passes the cavity. The phase at which the energy gain in the RF cavity equals the energy loss per turn U_0 is referred to as the *synchronous phase* ϕ_s. We can then write

$$\Delta U = qV_0 \sin(\phi_s - \omega_{RF} t) \stackrel{!}{=} U_0. \tag{I.14.39}$$

The synchronous phase depends on the charge of the particles and the amount of energy emitted. For positively charged hadrons, the energy loss is only significant at high energies in the TeV range. The synchronous phase is thus slightly below π as illustrated in Fig. I.14.17a. In the case of negatively charged electrons with a large energy loss per turn, shown in Fig. I.14.17b, the synchronous phase is in the range from $3\pi/2$ to 2π.

Question I.14.11: As Fig. I.14.17 indicates, there are always two phases satisfying Eq. (I.14.39). Can you specify under which conditions either of the solutions is applied?

I.14.6.4 How many RF cavities do we have to install? What voltage is required?

Concerning the design of the RF sections, we already discussed in Section I.14.6.1 that a well distributed high number of RF sections helps to reduce the amplitude of the sawtooth orbit. Not only the localisation of the RF sections, but also the choice of the total RF voltage, necessitate certain considerations: Obviously, the sum of all RF cavity voltages in the storage ring has to be larger than the energy loss per turn divided by e, otherwise the particle energy cannot be restored. Another important aspect to consider is the RF acceptance, which is directly affected by the value of the RF voltage. The RF acceptance is defined by the maximum momentum deviation a particle can assume without leaving the stable area in

longitudinal phase space, the so-called RF bucket, and can be defined by [8]

$$\delta_{\mathrm{RF}} = \frac{2Q_s}{h|\eta|}\sqrt{1+\left(\phi_s-\frac{\pi}{2}\right)\tan\phi_s}, \tag{I.14.40}$$

where h is the harmonic number, η the phase slip factor (see Chapter I.4 on longitudinal beam dynamics) and Q_s is the synchrotron tune

$$Q_s = \frac{1}{2\pi}\sqrt{-\frac{eV_{\mathrm{RF}}}{cp_0}\frac{\omega_{\mathrm{RF}}C}{c}\eta\cos\phi_s} \propto \sqrt{V_{\mathrm{RF}}}. \tag{I.14.41}$$

Combining Eqs. (I.14.40) and (I.14.41) reveals that the RF acceptance is proportional to the square root of the RF voltage, $\delta_{\mathrm{RF}} \propto \sqrt{V_{\mathrm{RF}}}$. Providing just sufficient RF voltage to exactly compensate for the energy loss (i.e., $\phi_s \to \pi/2$), the RF bucket becomes infinitesimally small and only particles with exactly the design momentum could be stored in the bucket as $\delta_{\mathrm{RF}} \to 0$. In order to allow phase focusing and stable storage of particles with a certain momentum deviation, the RF voltage has to be increased. This is of particular importance for light sources, which commonly operate in the low GeV energy range, where lifetime is limited by the Touschek effect. The Touschek effect describes the scattering of two particles in the bunch resulting in a transfer of transverse momentum to longitudinal momentum. If the longitudinal momentum gain is larger than the momentum acceptance, the particle is kicked out of the bucket and, in case of an electron storage ring, would be lost. In the ideal case, the RF voltage is set to such a high value that the RF acceptance is larger than the momentum acceptance imposed by lattice and optics.

I.14.6.5 Could you give an example of how the RF cavities are integrated on site?

High performance cavities have a superconducting surface coating and therefore have to be installed in a cryomodule that usually contains several cavity units. The cryomodule currently foreseen for the 400 MHz cavities of FCC-ee has a length of about 12 m and will contain four two-cell cavities [27] as illustrated in Fig. I.14.18. In the RF section the FODO cell length is increased to about 100 m. In-between two quadrupole magnets four cryomodules will be installed resulting in eight cryomodules per FODO cell [28]. Civil engineering has to include caverns for the cryoplants that supply the cryomodules with liquid helium and klystron galleries where the RF power is generated. As an example, the tunnel cross section proposed for the FCC-ee RF section is shown in Fig. I.14.19 [28]. From lattice design point of view, dispersion-free straight sections have to be included, where the cavities are installed.

I.14.6.6 Why do RF cavities have to be installed in dispersion-free sections?

RF cavities have to be installed in dispersion-free sections of the ring to avoid coupling between the longitudinal motion (energy) and the transverse motion via dispersion. Otherwise, so-called synchrobetatron resonances are excited, if following condition for the tunes is fulfilled

$$mQ_x + nQ_y + lQ_s = \text{integer} \qquad \text{with } m,n,l \in \mathbb{N}. \tag{I.14.42}$$

Synchrobetatron resonances reduce lifetime drastically and therefore limit the performance of storage rings [19].

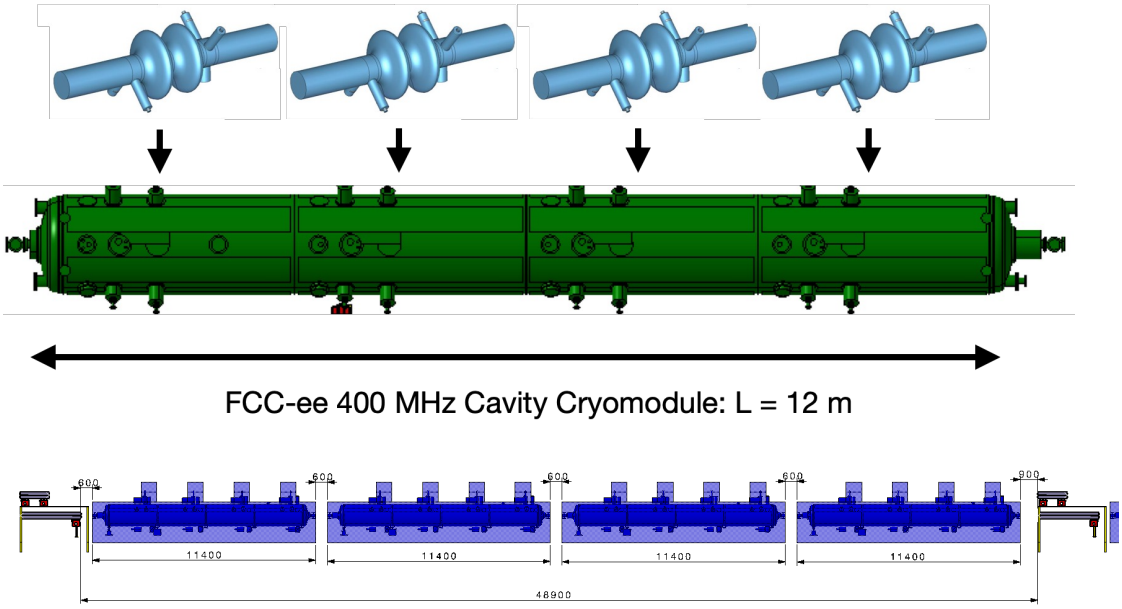

Fig. I.14.18: The figure shows a drawing of a cryomodule for four 400 MHz two cell cavities as foreseen for FCC-ee [27, 28]. In-between two quadrupole magnets four cryomodules will be installed.

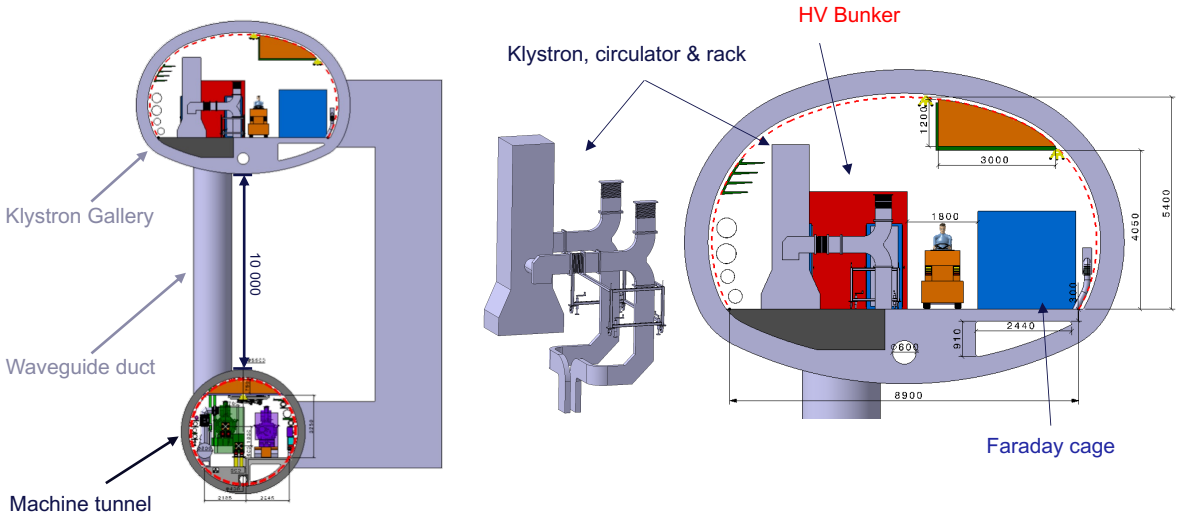

Fig. I.14.19: This picture shows an illustration of the tunnel cross section of the RF section proposed for FCC-ee [28]. Above the collider tunnel a separate tunnel housing the klystron gallery is foreseen.

I.14.7 Step V: Dispersion suppressors

Open the arc lattice to install straight sections for RF, interaction regions and or other insertions. Install dispersion suppressors to match the dispersion function to zero.

This sections discusses how dispersion-free sections can be obtained in a storage ring in case the basic cell is not achromatic. For details about the dispersion function, see the Chapter I.3 on transverse beam dynamics. Dispersion suppressor concepts are for example discussed in the references [7, 9, 10, 19, 29].

I.14.7.1 Remind me: what is dispersion in context of particle accelerators?

The equation of motion for a particle with ideal momentum is given by Hill's equation, which is a homogeneous differential equation. In case the particle has a momentum offset, an additional term is added on the right hand side and the equation becomes inhomogeneous:

$$x'' + x\left(\frac{1}{\rho^2} - k_1\right) = \frac{\Delta p}{p_0}\frac{1}{\rho}. \tag{I.14.43}$$

The solution for the transverse position is given by the sum of the homogeneous solution $x_\beta(s)$ and the particular solution $x_\delta(s)$ as stated in Eq. I.14.36. The dispersion function is then defined as the particular solution of the inhomogeneous Hill's equation normalised to the relative energy offset δ

$$D_x(s) = \frac{x_\delta(s)}{\delta}. \tag{I.14.44}$$

It can be understood as a special orbit a particle with $\delta = 1$ would have. Clearly, particles with $\delta = 1$ could not be stored in the storage ring. Typical values for the energy offset are $\delta \approx 10^{-3}$. At a position where the dispersion function has a value of $D = 1\,\mathrm{m}$ the orbit offset would then be $x_\delta = 1\,\mathrm{mm}$.

As particles with energy offset take a different orbit with a larger transverse amplitude, dispersion contributes to the beam size

$$\sigma_x(s) = \sqrt{\epsilon_x \beta_x(s) + D_x^2(s)\delta^2} \quad . \tag{I.14.45}$$

As a consequence, the dispersion functions have to vanish at positions where minimum beam sizes are required, as for example the interaction point of a collider.

Question I.14.12: We already discussed that the dispersion function needs to vanish in RF cavities (to prevent synchro-betatron resonances) and at collision points of colliders. If you think about light sources, why do you think undulators should be installed in dispersion-free sections as well?

I.14.7.2 What is the basic idea of a dispersion suppressor and when do we need it?

Light sources usually have achromatic lattices, which means the dispersion function and its derivative vanish at the beginning and at the end of the cell. In this case no extra measures have to be taken. Particle colliders on the other hand with high-energy beams are built of FODO cells, where the dispersion function is non-zero everywhere if bending magnets are installed.

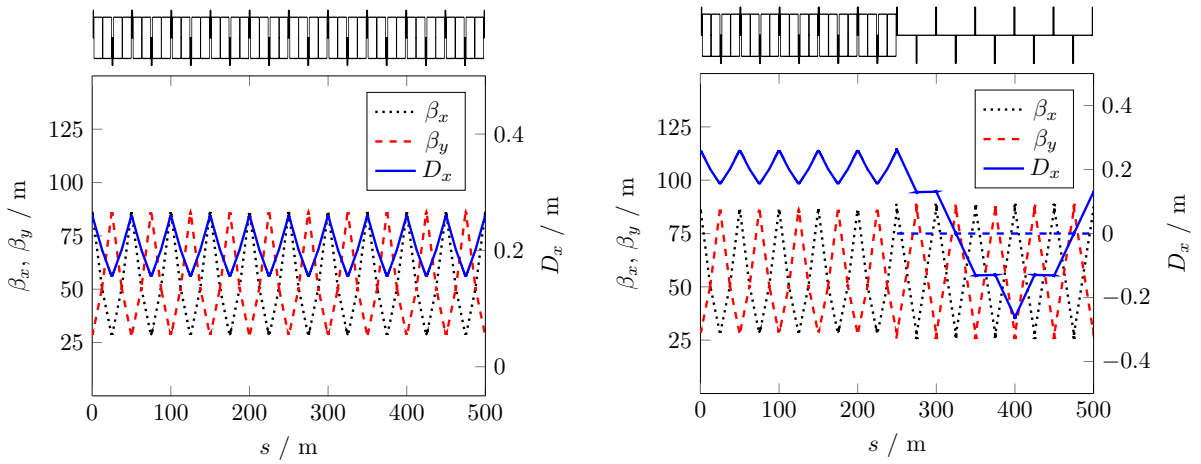

Fig. I.14.20: (a) Ten FODO cells in an arc section with 50 m length and 60° phase advance in both planes. The dispersion function oscillates regularly in phase with the horizontal β-function. (b) Example of an unmatched 60° optics: instead of following the periodic solution of the straight FODO cells indicated by the dashed line, the dispersion function starts beating in the absence of the bending magnets. Such an optics does not permit the installation of RF cavities or interaction regions.

Figure I.14.20a shows a toy FODO lattice consisting of ten arc cells with a length of 50 m each and a 60° optics. The periodic solution of the dispersion function shows a regular oscillation in phase with the horizontal β-function. As already discussed in Section I.14.5.8, the maximum an minimum values of the dispersion function can be calculated analytically and depend on cell length, bending radius and phase advance. In FODO cells of a straight section without any dipole magnets the periodic solution of the dispersion function is zero. If arc and straight section FODO cells would just be attached to each other, the transition from the arc to the straight cell solution would be unmatched. As long as the weak focusing of the dipoles is negligible the β-functions are not disturbed, but the dispersion function starts beating around the periodic solution as illustrated in Fig. I.14.20b. Such an optics does not permit the installation of RF cavities or interaction regions, as the condition $D_x = D'_x = 0$ is not fulfilled. In order to have a smooth transition from the oscillating solution of the arc sections to the zero-solution of the straight cells, a lattice section has to be installed that matches the dispersion function of the arc cells with the one of the straight cells. Such an insertion is called a *dispersion suppressor* as it brings the non-zero dispersion function to zero. Depending on the arc layout and given boundary conditions different arrangements of magnets can be chosen to design a dispersion suppressor:

- **Quadrupole-based schemes:** Since dispersion is "only another orbit" quadrupoles can be used to match dispersion;
- **Dipole-based schemes:** It is the dipoles that introduce dispersion in the first place. Clever arrangements can be used to suppress it again;
- **Combined schemes:** Of course both concepts can be combined to comply with certain boundary conditions or for larger flexibility.

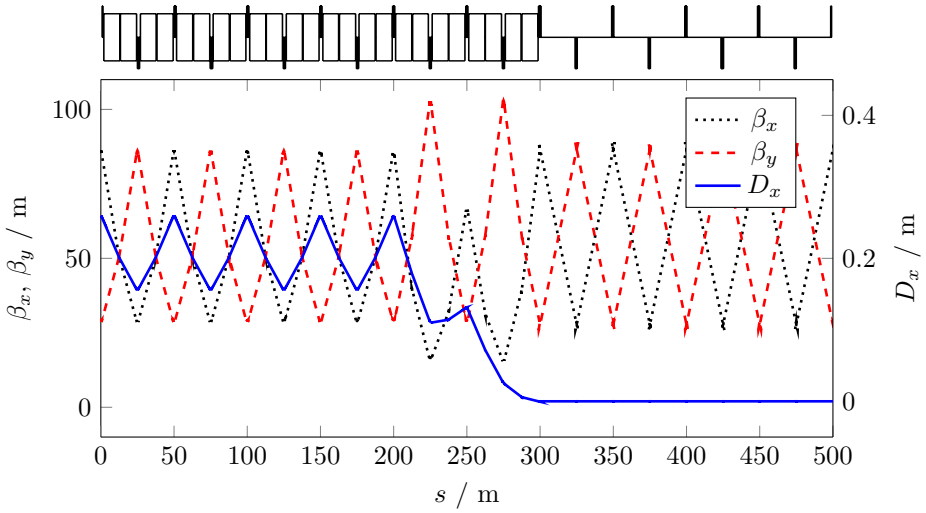

Fig. I.14.21: Transition of an arc section into a straight section using a quadrupole-based dispersion suppressor. In the last two arc cells the effect on the β-functions is visible.

I.14.7.3 Tell me more about quadrupole-based dispersion suppressors!

The dispersion function D_x and its derivative $D'_x = \mathrm{d}D_x/\mathrm{d}s$ can be suppressed solely by matching the strengths of quadrupole lenses. This scheme of dispersion suppressor can be considered as "the straight forward one" since the quadrupoles of the cells in the transition region between arc and straight sections usually are equipped with individual power supplies and no other measures have to be taken concerning the magnetic lattice and the cell design. However, quadrupoles also have an influence on the optics functions and thus the phase advance. As a consequence, also the β-functions (β_x and β_y) and α-functions (α_x and α_y) have to be re-matched, which means at least six individually powered quadrupoles are needed for this scheme. If also phase advances should be matched, additional quadrupoles have to be included. An example is given in Fig. I.14.21 for a lattice consisting of 50 m long FODO cells and a 60° optics. The last six quadrupoles of the arc section have been powered individually and their strengths have been matched to suppress the dispersion and its derivative while restoring the optics in the cells of the straight section. Figure I.14.21 also shows the effect on the β-functions resulting from the matching of the quadrupole strengths.

Advantages of the quadrupole-based dispersion suppressor scheme are:

+ It is easy to implement;
+ The geometry of the ring is not affected;
+ It is a flexible scheme that works for any phase advance per cell;
+ It can be used to connect different lattice structures and/or cells with different phase advances.

Challenges coming with the quadrupole-based dispersion suppressor scheme are:

– Many additional power supplies are required (expensive);
– The individual strength of the quadrupoles can be higher, which might require a different hardware design;

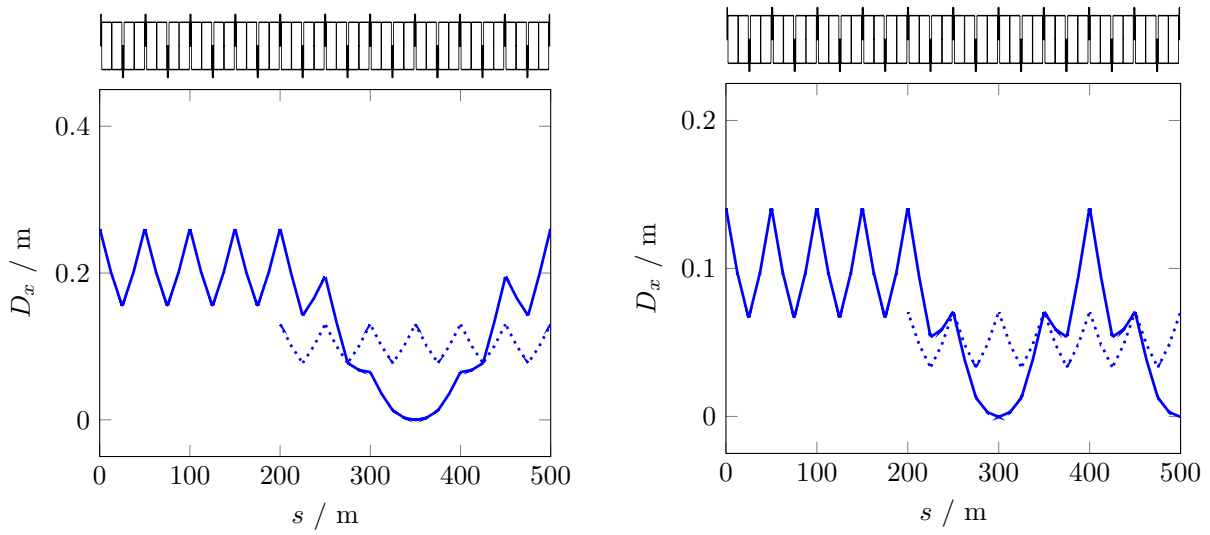

(a) 60° optics

(b) 90° optics

Fig. I.14.22: Illustration of the underlying principle of the half-bend dispersion suppressor scheme in a toy lattice consisting of four regular arc cells and six half-bend cells: the dispersion function starts to beat around the periodic solution in the half-bend cells, indicated by the dotted line, as soon as the half-bend cells are reached. It requires a phase advance of 2π for one oscillation. At the point where $D_x = 0$ and $D' = 0$ the half-bend cells will be cut off and replaced by the empty FODO cells of the straight section.

- The optics is affected. Tunes or local phase advances might have to be restored;
- Depending on number and distance of the used quadrupoles, the β-function might reach high values that require a modification of the vacuum chamber for larger aperture.

I.14.7.4 Tell me more about the half-bend dispersion suppressor!

Dipole-based dispersion suppressors are the most elegant way to match the dispersion to zero as long as the boundary conditions allow to implement such a scheme. As the name already says, a half-bend dispersion suppressor consists of FODO cells with bending magnets of exactly half the bending angle compared to the dipoles in the regular arc cells. As a consequence of Eq.s (I.14.28), the minimum and maximum values of the periodic solutions are half. If now the half-bend cells are attached to the regular arc cells, the transition of the dispersion function from the periodic solution of the arc is mismatched to the one in the half-cells. As in case of the straight cells, the dispersion function begins to beat. The difference between the two cases is the amplitude of the beating: for the half-bend cells the values oscillate between $D_x = \hat{D}_x$ and $D_x = 0$ instead of $D_x = \hat{D}_x$ and $D_x = -\hat{D}_x$. Figure I.14.22 illustrates the dispersion beat both for a 60° optics (a) and a 90° optics (b). The periodic solutions in the half-bend cells are again indicated by the dotted line. Also important to note is the period length of the beating: comparing Fig. I.14.22a and Fig. I.14.22b shows that the period length depends on the FODO cell phase advance. It requires a phase advance of 2π to complete one period: for a phase advance of $\varphi_x = 60°$ per FODO cell the period length is six cells, for a phase advance of $\varphi_x = 90°$ it is four cells. Still, for both the 60° and the 90° optics locations can be identified, where $D_x = 0$ and $D' = 0$: for the 60°

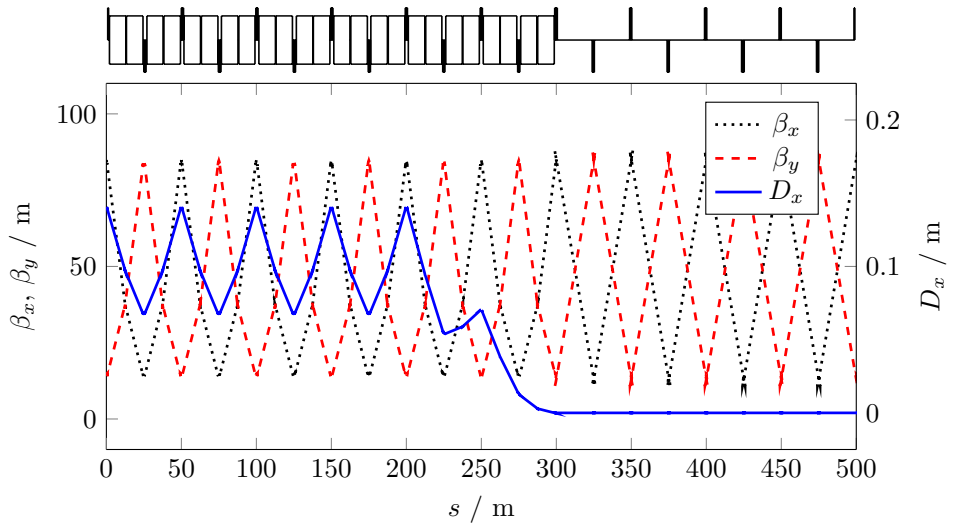

Fig. I.14.23: Transition of an arc section to a straight section using a half-bend dispersion suppressor to match the dispersion function. In-between four arc cells with 90° optics and four straight cells two half-bend cells serve as dispersion suppressor. The dispersion function starts beating as soon as the half-bend cells are reached. After the two half-bend cells the dispersion and its derivative are suppressed without affecting the β-functions. The small differences of the β-functions in arc and straight section originate from the geometric focusing of the bending magnets in the arc section.

optics at $s = 350\,\mathrm{m}$ and for the 90° optics at $s = 300\,\mathrm{m}$. The idea is therefore to use this beating to suppress the dispersion function: after half an oscillation, where the dispersion function reaches zero, the half-bend cells are cut off and replaced by the straight section cells. Hereby, a matched optics is obtained as illustrated in Fig. I.14.23 for the example of a 90° optics. After two half-bend cells the dispersion reaches zero which corresponds to the periodic solution of the dispersion function in the straight section cells and dispersion beating is prevented. Since no quadrupoles have been involved, the β-functions are not affected by the half-bend dispersion suppressor.

The concept of the half-bend dispersion suppressor only works, if after a certain number of FODO cells the dispersion function really reaches zero. In other words, it only works for certain values of the FODO cell phase advance. In the remaining part of this section, the conditions are being discussed that have to be fulfilled for this scheme. For the derivation of these conditions and a detailed description of the mathematics behind dispersion suppression we refer to [29] or [9]. In general, the dispersion suppressor has to fulfill two requirements: Firstly, the dispersion function D_x has to be zero and, secondly, its derivative D_x' has to be zero. If we require $D_x = 0$ we get the condition

$$2\theta_{\mathrm{DS}} \sin^2\left(\frac{n\varphi_x}{2}\right) = \theta_{\mathrm{B}}, \tag{I.14.46}$$

where n is the number of FODO cells with reduced bending angle, θ_{DS} is the dipole bending angle in the dispersion suppressor cells and θ_{B} the bending angle in the arc cells. In case of the half-bend dispersion suppressor the bending angle $\theta_{\mathrm{DS}} = \theta_{\mathrm{B}}/2$ which simplifies Eq. (I.14.46) to

$$\sin^2\left(\frac{n\varphi_x}{2}\right) = 1. \tag{I.14.47}$$

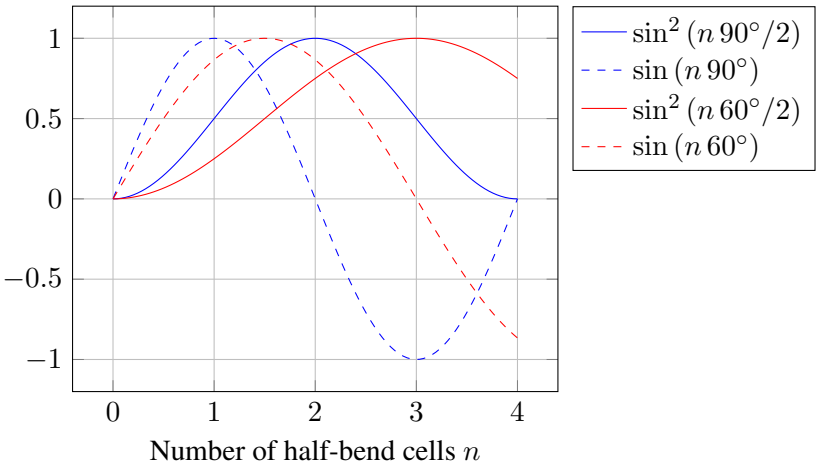

Fig. I.14.24: Plots of the angular functions in Eq. (I.14.47) and Eq. (I.14.48) for 90° and 60° phase advance per FODO cell depending on the cell number. For 90° phase advance both conditions are fulfilled for $n = 2$, for 60° for $n = 3$.

For $D'_x = 0$ the condition

$$\sin(n\varphi_x) = 0 \tag{I.14.48}$$

can be derived. Both conditions are fulfilled, if

$$n\varphi_x = k\pi \qquad \text{with} \quad k = 1, 3, \ldots\,, \tag{I.14.49}$$

or in words, when n half-bend cells have phase advance of an odd multiple of π. Figure I.14.24 shows the angular functions of Eq. (I.14.47) and Eq. (I.14.48) for the two examples of $\varphi_x = 90°$ and 60° FODO cell phase advance. For $\varphi_x = 90°$, the two conditions are fulfilled for $n = 2$, which means two half-bend cells have to be employed as discussed above. For $\varphi_x = 60°$, the conditions are fulfilled for $n = 3$, so three cells are required. More examples are provided in the summary table of Section I.14.8.

I.14.7.5 Are there more dipole-based schemes?

The half-bend dispersion suppressor is just one special set of solutions that match the dispersion function and its derivative to zero. A more general discussion, provided in [29], also leads to a different scheme, the *missing-bend scheme*. If the dipole strength in the suppressor cells does not have to be uniform, the dispersion function can for any phase advance be suppressed within two FODO cells, which in this context will be called *two-cell dispersion suppressor with diverse bending fields*.

I.14.7.5.1 Missing-bend scheme

The missing-bend scheme works similarly to the half-bend scheme. The dispersion suppressor consists of N cells in total. Instead of bending magnets at half field strength, the initial perturbation of the dispersion function is created by a number of m cells in which the dipoles are removed completely. Those cells are followed by n cells of uniform bending strength. The bending strength in those n cells can be the same as in the regular cells, but it also can be different.

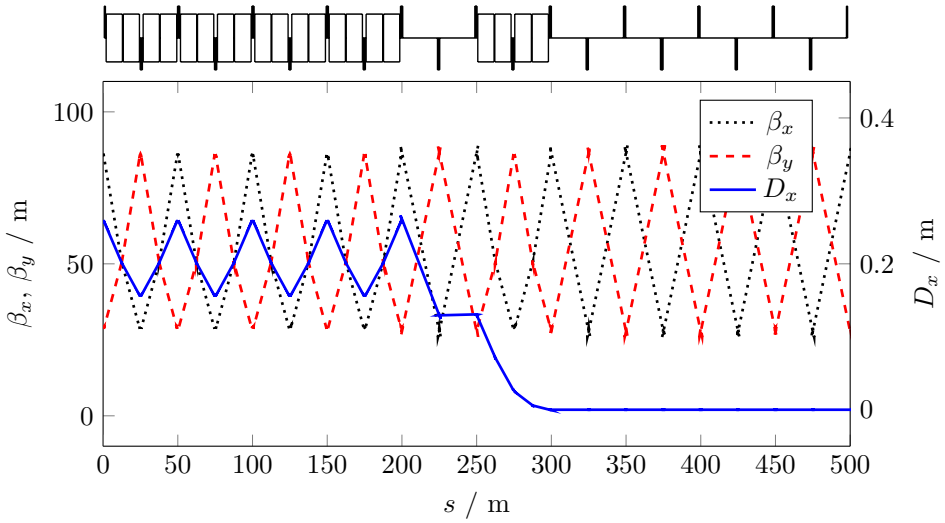

Fig. I.14.25: Transition of an arc section into a straight section in an example lattice consisting of 50 m long FODO cells with a 60° optics. A missing-bend dispersion suppressor scheme is used. Note the empty cell followed by one regular FODO cell.

As for the half-bend scheme, conditions can be derived for which dispersion and its derivative vanish. For the phase advance, the condition is

$$(2m+n)\varphi_x = (2k+1)\pi \tag{I.14.50}$$

and for the number of regular cells after the gap

$$\sin\frac{n\varphi_x}{2} = \frac{1}{2} \quad \text{for} \quad k = 0, 2, \ldots \qquad \text{or} \qquad \sin\frac{n\varphi_x}{2} = -\frac{1}{2} \quad \text{for} \quad k = 1, 3, \ldots \,. \tag{I.14.51}$$

An example of a missing-bend dispersion suppressor is shown in Fig. I.14.25, where the phase advance per cell is 60°. The gap consists of one empty FODO cell followed by one cell with bending magnets with the same strength as in the arc. As in case of the half-bend scheme, the β-functions are not affected here as the quadrupoles have not been touched. Solutions for other phase advances are provided in the summary table of Section I.14.8.

I.14.7.5.2 Two-cell dispersion suppressor scheme with diverse bending fields

The half-bend and missing-bend dispersion suppressors only work for specific values of the phase advance. In both schemes all dipoles of the suppressor section have a uniform strength. If instead different bending angles are allowed in the suppressor cells, the dispersion and its derivative can be suppressed within two cells for any FODO cell phase advance φ_x as long as the following conditions are fulfilled [19]

$$\theta_{\mathrm{B,A}} = \theta_{\mathrm{B}}\left(1 - \frac{1}{4\sin^2(\varphi_x/2)}\right), \quad \theta_{\mathrm{B,S}} = \frac{\theta_{\mathrm{B}}}{4\sin^2(\varphi_x/2)}. \tag{I.14.52}$$

Table I.14.5: Examples of bending strengths in the two-cell dispersion suppressor scheme for different FODO cell phase advances φ_x. θ_B is the nominal bending angle, $\theta_\mathrm{B,A}$ the one in the FODO cell next to the arc, $\theta_\mathrm{B,S}$ the one in the cell next to the straight.

φ_x	$\theta_\mathrm{B,A}/\theta_\mathrm{B}$	$\theta_\mathrm{B,S}/\theta_\mathrm{B}$	
108°	0.62	0.38	
90°	0.50	0.50	corresponds to half-bend scheme
76°	0.34	0.66	
60°	0.00	1.00	corresponds to missing-bend scheme
45°	-0.71	1.71	requires reverse bends and $\theta_\mathrm{B,S} > \theta_\mathrm{B}$

θ_B is the nominal bending strength of the regular arc dipoles, $\theta_\mathrm{B,A}$ is the strength of the dipoles in the FODO cell next to the arc cells and $\theta_\mathrm{B,S}$ is the one in the FODO cell next to the straight section. Table I.14.5 summarises the values of $\theta_\mathrm{B,A}$ and $\theta_\mathrm{B,S}$ for different phase advances. For $\varphi_x \leq \pi/3$ reverse bends with negative strength are used in the cell next to the arc cells. In addition, the bending strength in the other cell becomes larger than the nominal bending strength, which might be critical in case of superconducting magnets, where the nominal bending strength already is defined by the technical limits.

I.14.7.6 What are advantages and disadvantages of dipole-based schemes? When do we need hybrid schemes?

The big advantage of dipole-based dispersion suppressors is they do not affect the optics. Because of the large bending radius, the weak focusing effect of the dipoles is negligible and modifications of the bending strength has very little impact. Therefore, aperture requirements stay the same and no extra quadrupole hardware has to be designed. Moreover, the optics does not need to be re-matched and no additional power supplies are required for free quadrupoles. On the other hand, dipole magnets with modified field strength are required. The corresponding change of bending radius has a strong impact on the geometry of the ring, hence, dipole-based schemes need to be included to the design at an early stage. Dipole-based schemes are always optimised for one specific optics with specific phase advance per cell. An optics change leading to a different phase advance per cell would require different bending angles for dispersion suppression, which would imply a modification of the geometry. For simulations this is not a problem, but for a real machine the change of phase advance would imply major reconstruction work. If different optics are foreseen in operation, they already need to be taken into account during design phase. One may eventually require additional quadrupoles to remain flexible. This is where the hybrid schemes come into play. In general, one of the two dipole-based schemes (missing or half-bend suppressor) is combined with a certain number of individual quadrupole lenses to guarantee the flexibility of the system with respect to phase advance changes in the lattice, fine-tuning of optics and tune and to keep the size of the β-function moderate. Also, if the footprint of a new accelerator is pre-defined (e.g. in the case of an existing tunnel), the dipole-based schemes cannot be fully exploited and need to be supported by quadrupoles. For lepton storage rings, schemes with reduced field at the end of the arc sections are beneficial as they reduce the level of synchrotron radiation entering from the arcs into the straight section. This is of particular interest, if there is an experimental region in the straight section.

I.14.8 Summary: Dispersion suppressor schemes

Quadrupole-based scheme:

+ Easy to implement
+ Does not affect the geometry of the ring
+ Flexible scheme that works for any phase advance per cell
+ Can connect different lattice structures and/or cells with different phase advances
− Additional power supplies are required
− The quadrupole strength can be higher requiring a different hardware design
− Affects the optics: tunes or local phase advances might have to be restored
− Large β-function might require a modification of the vacuum chamber for larger aperture

Dipole-based schemes:

+ The optics is not affected as the quadrupoles are not touched
+ Reduced synchrotron radiation in the straight section due to reduced bending strength
− Affect the geometry thus not flexible for optics changes
− Half-bend and missing-bend scheme are optimised for specific values of the phase advance:

Phase advance φ_x	Suppressor cells N	Empty cells m	Cells with dipoles n	Bending angle θ_{DS}
108°	5	0	5	$\theta_{\mathrm{B}}/2$
90°	2	0	2	$\theta_{\mathrm{B}}/2$
60°	3	0	3	$\theta_{\mathrm{B}}/2$
45°	4	0	4	$\theta_{\mathrm{B}}/2$
60°	2	1	1	θ_{B}
45°	3	1	2	$\theta_{\mathrm{B}}/\sqrt{2}$
30°	4	2	2	θ_{B}
77°	4	3	1	-$\theta_{\mathrm{B}}/1.25$

Hybrid schemes:

✓ Combination of dipole-based scheme with additional quadrupoles
✓ Reduces the effect on the optics while maintaining flexibility for optics changes and fine-tuning
✓ Usually the way to go!

I.14.9 Step VI: Matching sections

Install matching sections where beam parameters have to be matched over short distances, such as at the transition of two different lattice structures, – and match the optics.

In this section we mainly discuss the use case of matching sections and a few examples. For a more detailed discussion including analytic solutions that can be of considerable help in guiding numeric matching routines see for example [29].

I.14.9.1 What is a matching section and what do I need it for?

Each periodic lattice structure has its periodic solution for the optics functions. Whenever we combine two different lattice structures we need a matching section in between to adapt the optics functions between the two lattices from one periodic solution to the other. Examples are the end of a transferline, low-beta insertions in colliders and the interface of arc and straight sections. In the matching section the quadrupoles are powered individually to allow individual strengths. The magnetic lattice itself can but does not need to be altered.

I.14.9.2 Can you give us some examples?

Figure I.14.26a shows the end of an arc section and the beginning of a straight section in an early lattice version of FCC-ee. The cell length is $54\,\mathrm{m}$ in the arc and $50\,\mathrm{m}$ in the straight section. The phase advance per cell is $\varphi_x = 90^\circ$ and $\varphi_y = 60^\circ$ in both arc and straight section. The last two cells of the arc section are half-bend cells to suppress dispersion (blue background). The five quadrupoles of the first three straight cells are powered individually (brown background). This is the matching section that is used to match the optics from the $54\,\mathrm{m}$ cell to the $50\,\mathrm{m}$ cell, which can be recognised at about $s = 480\,\mathrm{m}$, where the vertical β-function is slightly larger than before.

The same lattice is shown in Fig. I.14.26b now with a $60^\circ/60^\circ$ optics. In this case the two half-bend cells are not sufficient anymore to suppress the dispersion function. Now the dispersion suppressor is supported by additional four individually powered quadrupoles leading to the irregular oscillation of the β-functions in the blue deposited area.

Figure I.14.27 shows a similar but more complicated example from an early lattice of the FCC-ee top-up booster synchrotron. Its footprint follows the layout of FCC-hh. The fixed length of the arc section with bending radius of $\rho = 13.15\,\mathrm{km}$ and the required values for the beam emittance lead to a cell length of $54\,\mathrm{m}$ that applies for the first five cells until the first blue vertical line. FCC-hh foresees a hybrid bend-quadrupole dispersion suppressor scheme with a length of $566\,\mathrm{m}$ and a larger bending radius of $\rho = 15.06\,\mathrm{m}$ (until second vertical blue line). In order to fit the tunnel geometry and the section length, the cell length has to be increased to $56.6\,\mathrm{m}$. In the following straight section a cell length of $100\,\mathrm{m}$ was chosen to allow for more space for the cryomodules of the RF cavities. The first two cells of the straight section have an intermediate length of $75\,\mathrm{m}$ to support the matching of the optics functions in the transition region. In summary: there are three different types of FODO cells and the optics has to be matched several times including the suppression of the dispersion function.

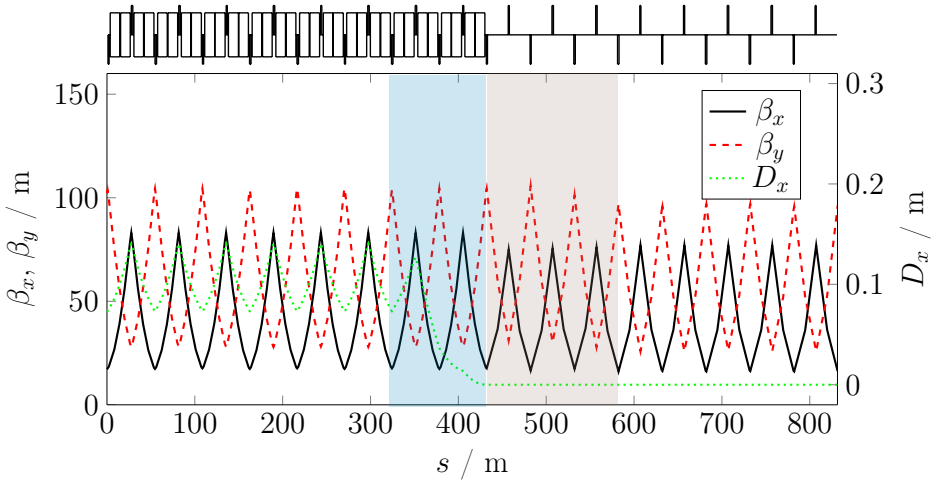

(a)

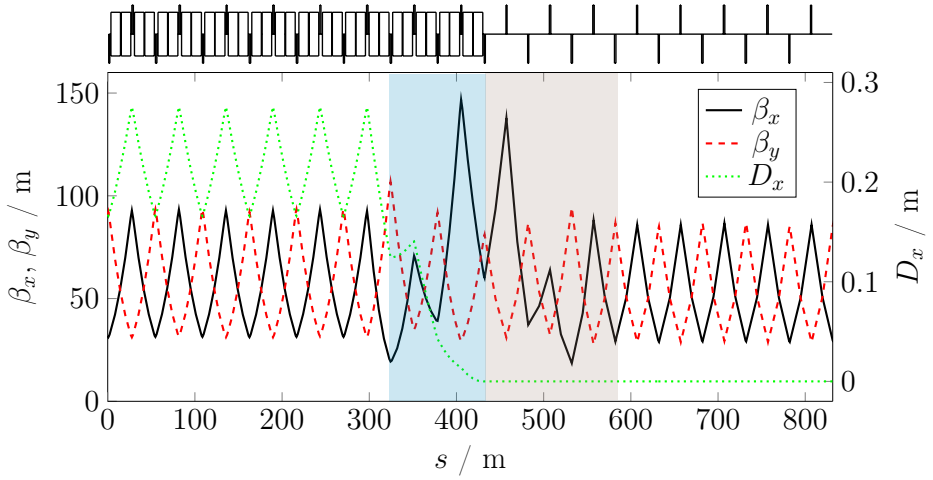

(b)

Fig. I.14.26: Examples for transitions from an arc section into a straight section. Plot (a) shows a 90° optics. The last two cells of the arc consist of two half-bend cells to suppress dispersion (blue background). Since the cell length is 54 m in the arc and 50 m in the straight section a matching section consisting of five individually powered quadrupoles (brown background) is used to match the optics. (b) shows the same lattice with a 60° optics. In this case three half-bend cells would be needed to suppress dispersion, therefore four additional free quadrupoles in the dispersion suppressor support the matching of the optics.

The first matching section is located in the first three of the 56.6 m cells (brown background) consisting of six individually powered quadrupoles to match $\beta_{x,y}, \alpha_{x,y}, D_x$ and D'_x. The last four cell of the arc are work as a quadrupole-based dispersion suppressor consisting of eight individually powered quadrupoles (blue background). In principle, the number of quadrupoles would be sufficient to again match six parameters. However, since the FODO cells of arc and straight section are very different in length and thus have very different periodic solutions, the minimum number of quadrupoles would lead to large values of the β-functions in the transition region. To reduce their values with respect to aperture requirements the additional matching section with intermediate cell length and additional four

quadrupoles has been added (brown background).

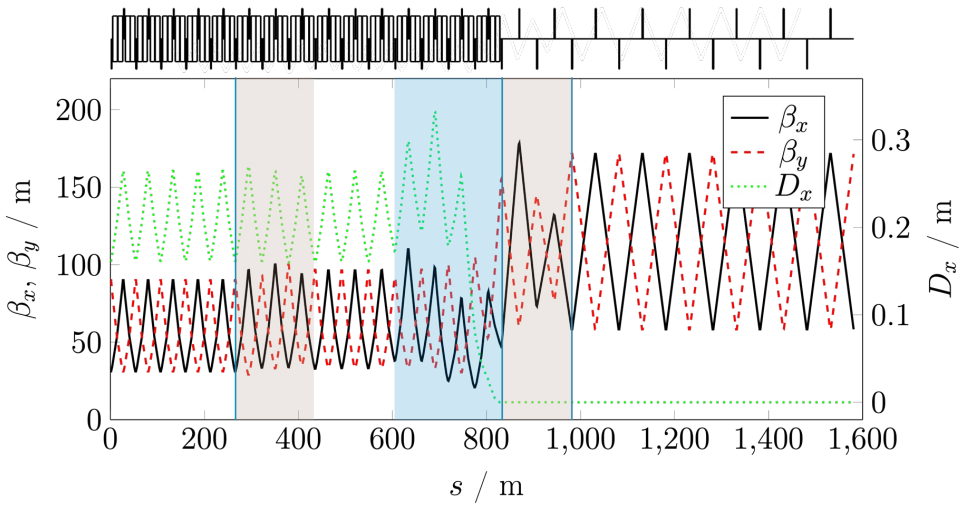

Fig. I.14.27: Transition region from the arc section to the RF straight section in an early version of the FCC-ee full-energy top-up booster synchrotron (adapted from [30]): different cell lengths require several matching sections (brown background) and a quadrupole-based dispersion suppressor (blue background). Details are described in the text.

Question I.14.13: What is the difference between a matching section and the quadrupole-based dispersion suppressor scheme we discussed earlier?

I.14.10 Step VII: Interaction regions

Install an interaction region, where the beams will be collided. An interaction region must be in a straight section that is dispersion-free and consists of a drift space for the detector, final focus quadrupoles to obtain minimum β-functions and matching sections on each side. Modern layouts, especially for linear colliders, also include local chromaticity correction schemes.

This section discusses the luminosity as the key performance parameter and the integration of interaction regions and related aspects that affect the design of interaction regions. More information on the lattice design of interaction regions can be found in [9] or [19].

I.14.10.1 Remind me: what is luminosity?

Luminosity is a measure for the number of particle collisions per area and time and is therefore one of the most important parameters of a particle collider. The production rate of a certain physics event is determined by the product of the event's cross section σ_p multiplied by the collider's luminosity $\mathcal{L}$

$$\frac{\mathrm{d}N_\mathrm{p}}{\mathrm{d}t} = \sigma_\mathrm{p}\mathcal{L}. \tag{I.14.53}$$

For head-on collision and Gaussian shaped bunches the luminosity is given by

$$\mathcal{L} = \frac{N_1 N_2 f n_\mathrm{b}}{4\pi\sigma_x^*\sigma_y^*} = \frac{1}{4\pi e^2 f n_\mathrm{b}} \frac{I_1 I_2}{\sigma_x^*\sigma_y^*}. \tag{I.14.54}$$

N_1 and N_2 describe the numbers of particles in the two colliding bunches. Alternatively, the bunch currents I_1 and I_2 can be used for the calculation. f is the revolution frequency and n_b is the number of bunches per beam. σ_x^* and σ_y^* are the transverse beam sizes at the interaction point. The design parameters of the LHC required for the calculation of the luminosity are summarized in Tab. I.14.6. According to Eq. (I.14.54) the LHC's head-on luminosity would be $\mathcal{L}_\mathrm{LHC,HO} = 1.16 \times 10^{34}\,\mathrm{cm}^{-2}$, slightly larger than the nominal luminosity of $\mathcal{L}_\mathrm{LHC} = 1.00 \times 10^{34}\,\mathrm{cm}^{-2}$, that includes the luminosity reduction due to the crossing angle at the interaction point (see Sec. I.14.10.2).

Table I.14.6: Summary of LHC parameters required for the calculation of the luminosity.

β-function at collision point	$\beta_{x,y}^*$	$0.55\,\mathrm{m}$
beam emittance	$\epsilon_{x,y}$	$5 \times 10^{-10}\,\mathrm{m}$
beam size at collision point	$\sigma_{x,y}^*$	$17\,\mu\mathrm{m}$
revolution frequency	f	$11.245\,\mathrm{kHz}$
number of bunches	n_b	2808
beam current	I	$584\,\mathrm{mA}$

Instead of the sometimes called *instantaneous luminosity* discussed above, often the *integrated luminosity* is mentioned. Luminosity integrated over time is a measure for the number of events produced

$$\mathcal{L}_\mathrm{int} = \int \mathcal{L}\,\mathrm{d}t = N_\mathrm{p}/\sigma_\mathrm{p}. \tag{I.14.55}$$

When knowing the integrated luminosity, multiplication with the cross sections allows to draw direct conclusions about how much data of a specific event is collected. As the cross section is a measure of the probability for the occurrence of a specific event, it is a constant value determined by the properties of the particles and interactions involved. Thus, for a higher production rate the luminosity has to be increased. Especially for the observation of rare decay events with very small cross sections, high luminosity is required to gain sufficient amount of statistics.

I.14.10.2 What are the steps to maximise luminosity? What are the limitations?

Recalling Eq. (I.14.54), the luminosity basically describes the density of the particle bunches at the collision point times repetition rate of bunch crossings. For highest luminosities, both particle density and repetition rate have to be as large as possible.

The repetition rate strongly depends on the geometry of the collider. In circular colliders, the repetition rate depends on revolution frequency and the number ob bunches per beam. In linear colliders, where the bunches only cross once, the repetition rate is determined by the potential of the injectors to produce new bunches. In a linear collider the repetition rate is typically in the range of $5\,\mathrm{Hz}$ to $100\,\mathrm{Hz}$ in contrast to tens of kHz in the case of circular colliders [31]. A related advantage of circular collid-

ers is that they can provide support several experiments at the same time. Operating two experiments at once doubles the crossing rate and thus also doubles the integrated luminosity. Moreover, if the experiments are conducted by different research collaborations using different detector designs, such as ATLAS and CMS at the LHC, they can cross-check their results and limit systematic effects in the measurement results. However, each additional experiment incurs costs for detector design and development, construction, staffing, operation and so on.

In case of circular colliders, the revolution frequency of the bunches is determined by the circumference of the storage ring. Therefore, in order to increase the repetition rate, the number of bunches must be maximised. A different layout choice sets the limit for this maximum: if a single vacuum chamber is used to store both beams, measures have to be taken to locally separate the bunches and prevent parasitic collisions outside of the detectors. The details of such separation schemes are beyond the scope of this discussion. Two separation schemes that have been implemented at LEP are for example described in [32]. Sticking to this example, the number of bunches in LEP was limited to 8 bunches per beam ($\mathcal{L} = 1.2 \times 10^{32}\,\mathrm{cm}^{-2}\,\mathrm{s}^{-1}$), while the double-ring collider LHC can store 2808 bunches per beam in the same tunnel ($\mathcal{L} = 1.0 \times 10^{34}\,\mathrm{cm}^{-2}\,\mathrm{s}^{-1}$). It has to be kept in mind, however, that with a high number of bunches the beams have to be collided at a crossing angle to avoid unwanted crossings in the part of the interaction region where the bunches share the vacuum chamber. A crossing angle reduces the bunch overlap and thus the luminosity. The calculation of the luminosity reduction factor is presented in [33]. At the LHC, a crossing angle of $285\,\mu\mathrm{rad}$ leads to a luminosity reduction of 0.835 and thus reduces luminosity from $\mathcal{L} = 1.2 \times 10^{34}\,\mathrm{cm}^{-2}\,\mathrm{s}^{-1}$ to $1.0 \times 10^{34}\,\mathrm{cm}^{-2}\,\mathrm{s}^{-1}$ [33].

Advanced crossing schemes aim to recover or even surpass the head-on luminosity. In this context, we would like to mention the *crab-crossing scheme* using crab cavities to rotate the colliding bunches, thereby increase the bunch overlap again and thus suppress luminosity loss. It will be implemented in the LHC high luminosity upgrade [34], for more information we refer to [35, 36]. Also, we would like mention the *crab-waist collision scheme*, which is considered attractive for future lepton storage-ring colliders, as it promises to suppress resonances and allows to increase luminosity by 1-2 orders of magnitude without increase in beam current or reduction of bunch length [37]. This scheme introduces large crossing angles ($30\,\mathrm{mrad}$ are proposed for FCC-ee [5]) and uses sextupoles to orient the beam waist at the interaction point along the trajectory of the other beam. Again, for detailed information we refer to publications such as [38–40].

As stated at the beginning of this discussion, besides the repetition rate the particle density must be maximised at the interaction point. There are two options for increasing the particle density: increasing the particles per bunch (*bunch population*), and decreasing the beam size. Particle colliders usually feature a bunch population in order of $\approx 10^{11}$ particles per bunch, which is the limit given by the beam-beam effect. The space charge of each of the colliding beams acts like a perturbing nonlinear lens to the respective other beam. There are numerous consequences from the beam-beam interaction, it may suffice here to mention two significant ones. First, the tunes of single particles will be shifted according to their amplitude within the nonlinear fields, which results in the beam-beam induced tune spread within a colliding bunch. This tune spread renders the bunch more susceptible to destructive betatron resonances surrounding the working point in the tune diagram. Second, the beam-beam force can drive the colliding bunches into coherent instability. A detailed discussion can be found e.g. in Ref. [41].

When discussing smallest beam sizes, several parameters are crucial: Firstly, the dispersion function must vanish at the interaction point. Dispersion contributes to the beam size and, if not eliminated, dilutes the luminosity. Additionally, non-zero dispersion during beam-beam interaction introduces synchro-betatron resonances [42, 43], which can affect beam quality and stability. Secondly, the beam emittance must be small, which is not straight forward to achieve. In the case of hadron storage rings, as previously discussed, the emittance is determined by the quality of the injectors. The high luminosity upgrade of the LHC therefore was preceded by the Large Injectors Upgrade (LIU) [44, 45] to reduce the normalised emittance from $3.75\,\mu\mathrm{m}$ to $2.50\,\mu\mathrm{m}$ [44]. In the case of lepton storage rings, the emittance is an equilibrium beam parameter and determined by the lattice design. It must therefore already be minimised during the design process. Later, there is no option anymore to decrease emittance except for minor modifications by increasing the phase advance per FODO cell and thus reducing the value of the dispersion function (see Eq. (I.14.28)).

Finally, the most important way to deliver small beam sizes and high luminosity when designing an interaction region is to strongly *squeeze* the β-functions to tiny sizes by focusing with strong quadrupole magnets. In the LHC, for example, the design values of the β-functions at the interaction point are $\beta^* = 0.55$ m in both planes. During the high-luminosity upgrade, they will be further reduced to $0.15\,\mathrm{m}$ [44]. For the FCC-ee, values in the range from $\beta_x^* = 0.15\,\mathrm{m}$ to $1.0\,\mathrm{m}$ are foreseen for the different operation modes and $\beta_y^* = 0.8\,\mathrm{mm}$ to $1.6\,\mathrm{mm}$ in the vertical plane. However, such strong focusing comes with significant challenges: The strong quadrupoles introduce substantial chromatic effects resulting in large values of the chromaticity. Special chromaticity compensation schemes need to be developed to correct the chromaticity without reducing the dynamic aperture by the nonlinear fields of the sextupoles. In addition, strong focusing results in highly divergent beams leading to large beam sizes that have to be accommodated in the vacuum chamber without aperture issues (see Sections I.14.10.4 and I.14.10.5).

One last thought: after continually increasing the luminosity, it is important to consider a limitation introduced by the detectors: the *pile-up* of events. The larger the luminosity, the higher is the probability for several collision per bunch crossing. In lepton colliders, usually only few events occur per bunch crossing because of the comparably low cross sections. In the case of proton collisions, however, the larger cross section leads to multiple interactions. In the LHC on average 20 events are expected per bunch crossing [33], but also crossings with more than 100 proton-proton interactions have already been observed [46]. As illustrated in Fig. I.14.28, the more interactions occur the more tracks are recorded and thus the more difficult becomes the reconstruction of the events from the detector signals. The detector performance consequently puts a limit on the pile-up and thus to the luminosity. If the luminosity surpasses the detector's capabilities luminosity leveling techniques can be employed. These techniques artificially decrease and control the luminosity by introducing a beam offset during collisions or by adjusting the β^* squeeze for example.

I.14.10.3 What is the layout of a typical interaction region?

At the center of the interaction region is the interaction point, where the two beams collide. This interaction point must be located in a drift space long enough to accommodate the detector. The ATLAS detector in the LHC, for example, has a length of $46\,\mathrm{m}$. The distance from the interaction point to the first

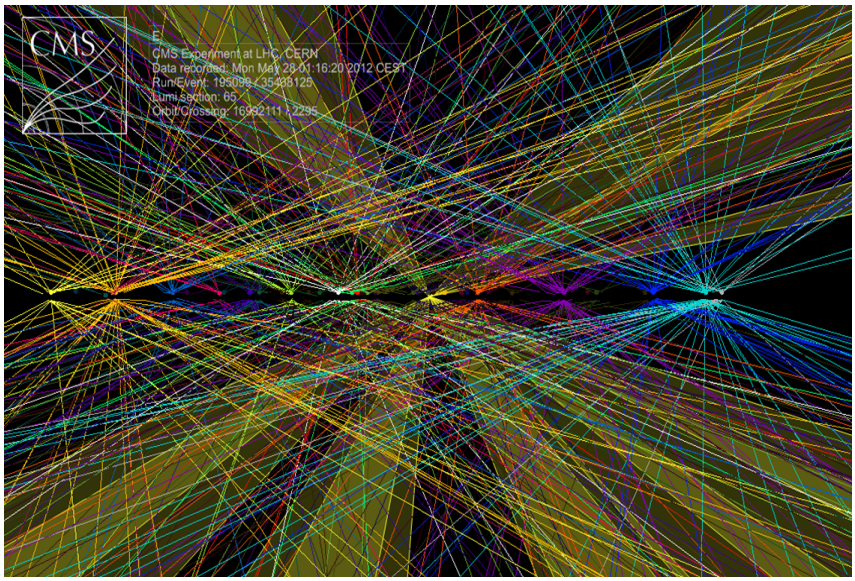

Fig. I.14.28: Tracks of charged particles close to the vertex region. Tracks that origin from the same interaction are coloured the same [46].

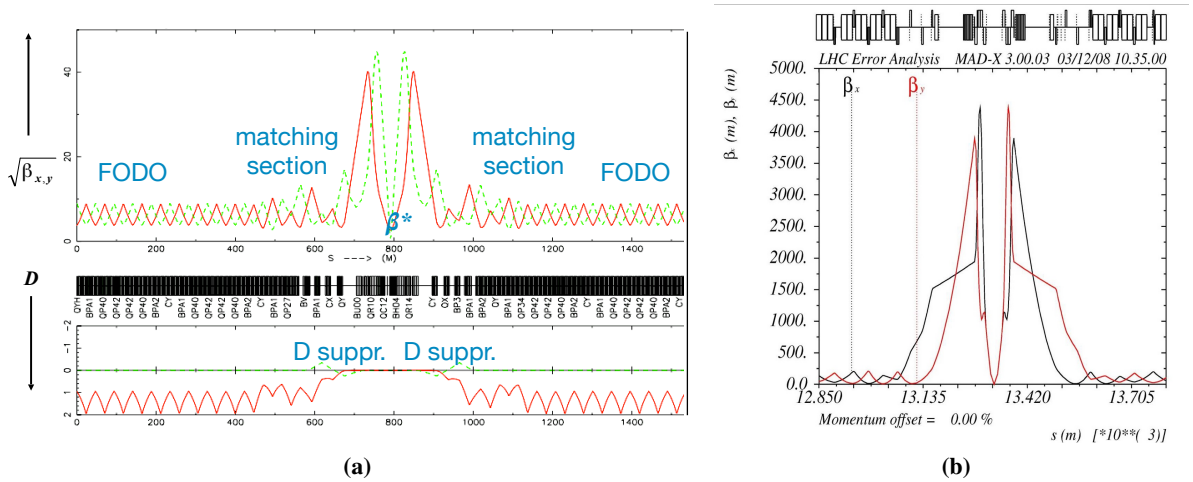

(a) **(b)**

Fig. I.14.29: (a) Interaction region layout and optics functions of the former electron-proton collider HERA at DESY, (b) High-luminosity interaction region of the hadron collider LHC at CERN.

quadrupole is therefore 23 m on each side. The strong focusing required for high luminosity is achieved using a doublet or triplet of quadrupoles, known as the *final focus quadrupoles*. In order to match the optics, matching section and dispersion suppressor are needed on each side before entering the arc section. Figure I.14.29 shows two examples of interaction regions with this layout: Figure I.14.29a shows the interaction region of the former electron-proton collider HERA at DESY, Fig. I.14.29b an interaction region of the hadron collider LHC at CERN.

Question I.14.14: In case of the HERA interaction region the β-functions are symmetric on both sides of the interaction point – $\beta_{x,y,}(s) = \beta_{x,y}(-s)$, in case of LHC they are asymmetric – $\beta_{x,}(s) = \beta_y(-s)$ and vice versa. Can you explain why?
Hint: HERA collided electrons and protons, LHC has proton-proton collisions.

Question I.14.15: In the interaction regions of some colliders the final focus quadrupoles consist of a doublet, in others they are a triplet. Do you have an idea why this is the case?

I.14.10.4 Why do the β-functions increase so much in the vicinity of the interaction point?

The increase of the beta functions in interaction regions is a direct consequence of Liouville's theorem, which states that the local particle density in phase space stays constant under the influence of conservative forces. This means that if the beam has been squeezed to a tiny size for high local particle density at the interaction point it is highly divergent. For linear motion, this can easily be illustrated looking at the equation of the beam emittance. As the interaction point is in the middle of a straight section and a symmetry point of the β-functions, $\alpha^* = 0$ and $\gamma^* = 1/\beta^*$. The equation of the emittance thus simplifies to

$$\epsilon(s) = \gamma(s)x^2(s) + 2\alpha(s)x(s)x'(s) + \beta(s)x'^2(s) = \frac{x^2}{\beta^*} + \beta^* x'^2. \tag{I.14.56}$$

Largest divergence is obtained for $x = 0$ given by $\sigma' = \sqrt{\epsilon/\beta^*}$. This clearly shows, that while small β-functions help to reduce the beam size $\sigma = \sqrt{\epsilon\beta}$, they increase the divergence.

The evolution of the optical functions from the interaction point to the first final focus quadrupole can be calculated using the matrix formalism. The transfer matrix corresponds to that of a drift space

$$M_{\text{drift}} = \begin{pmatrix} m_{11} & m_{12} \\ m_{21} & m_{22} \end{pmatrix} = \begin{pmatrix} 1 & s \\ 0 & 1 \end{pmatrix}. \tag{I.14.57}$$

Given the elements m_{ij} of the transfer matrix, the optical functions at position s_1 can be transformed to the corresponding functions at position s_2 as follows

$$\begin{pmatrix} \beta \\ \alpha \\ \gamma \end{pmatrix}_{s_2} = \begin{pmatrix} m_{11}^2 & -2m_{11}m_{12} & m_{12}^2 \\ -m_{11}m_{21} & m_{12}m_{21} + m_{11}m_{22} & -m_{12}m_{22} \\ m_{12}^2 & -2m_{22}m_{21} & m_{22}^2 \end{pmatrix} \begin{pmatrix} \beta \\ \alpha \\ \gamma \end{pmatrix}_{s1}. \tag{I.14.58}$$

In this case, the interaction point is at $s_1 = 0$ which means for the optical functions $\alpha(s_1) = \alpha^* = 0$ and $\gamma(s_1) = 1/\beta(s_1) = 1/\beta^*$. With those assumptions, expanding Eq. I.14.58 yields following expression for the evolution of the β-function in the drift space between interaction point and final focus quadrupole

$$\beta(s) = \beta^* + \frac{s^2}{\beta^*}. \tag{I.14.59}$$

As illustrated in Fig. I.14.30, the β-function has the shape of a parabola with its minimum value β^* at

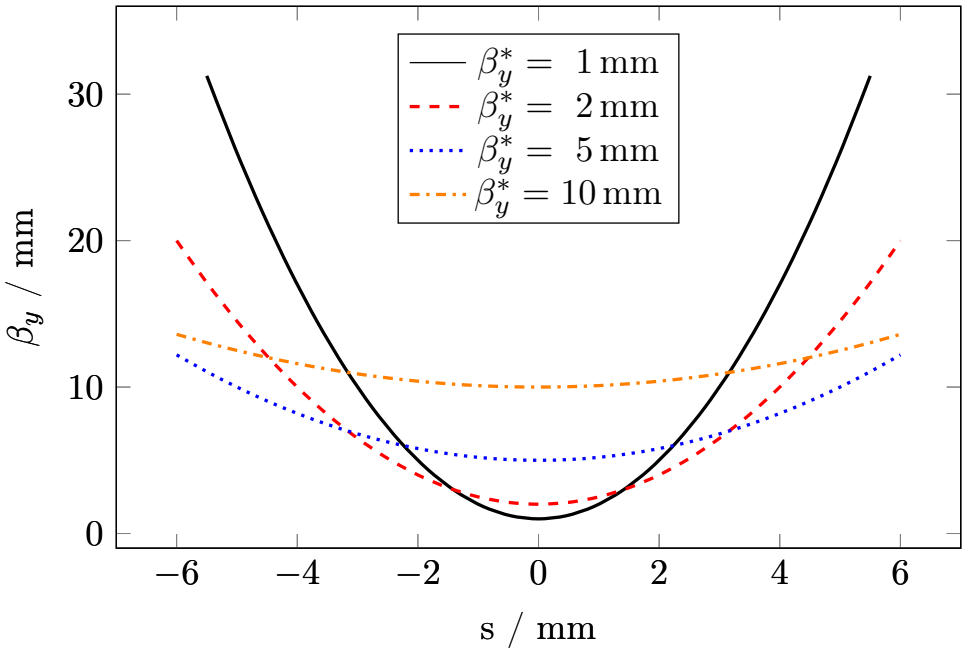

Fig. I.14.30: The β-function in the vicinity of the interaction point at $s = 0$ for different values of β^* [12]. The β-function increases quadratically with distance s. The smaller β^*, the larger becomes the beam divergence.

the interaction point at $s = 0$. The smaller β^* becomes, the faster the β-functions increase with distance from the interaction point. The only possible means to limit the growth of the β-functions is to keep the distance from interaction point to the first final focus quadrupole, usually denoted as L^*, as small as possible and to not reduce β^* any further.

Question I.14.16: Contextualise the quadratic increase of the β-function in a drift section. Does this make sense, if you think about the trajectory of a particle in a drift space? What does this mean for the beam size?

I.14.10.5 Are there special requirements on the final focus quadrupoles?

The final focus quadrupoles must meet extremely high requirements. Primarily, they need to be very strong to achieve the necessary focusing at the interaction point. The quadrupole gradient g is determined by the pole tip field B, i.e. the magnetic field at the pole surface, and the aperture radius r

$$g = \frac{\mathrm{d}B}{\mathrm{d}r}. \tag{I.14.60}$$

This means that for large gradients, a small aperture radius is beneficial. However, as discussed above, the β-functions increase rapidly near the interaction point, leading to large beam sizes and the largest aperture requirements in the entire storage ring. If the quadrupoles use superconducting coils, additional shielding may be required to protect the superconductor from energy intake and mechanical damage caused by collision debris. This shielding further reduces the available aperture. If the requirements on

the optics are very aggressive, demanding smallest values of β^*, one solution is to reduce the distance to the interaction point L^* and install the final focus quadrupoles inside the detector. This approach imposes spatial constraints: the solid angle occupied by the magnets, i.e. the blind spot of the detector, should be as small as possible, necessitating very compact, superconducting designs. In the case of FCC-ee, L^* has a value of $2.2\,\mathrm{m}$ and the magnet system consisting of final focus quadrupoles and compensating solenoid must not exceed an angle of $\pm 100\,\mathrm{mrad}$ within the detector [5]. This discussion illustrates that design and placement of the final focus quadrupole require a compromise between achievable quadrupole gradient, available aperture, and distance to the interaction point.

However, there are not only special requirements on the design of the quadrupoles but also on their performance and quality. Their quadrupole strength k_1 must fulfill highest precision requirements, because the tune shift created by a gradient error,

$$\Delta Q = -\frac{1}{4\pi}\beta(\tilde{s})\Delta k_1 L_\mathrm{Q}, \tag{I.14.61}$$

scales with the β-function at the position $\tilde{s}$ of the perturbed quadrupole. As the β-functions reach values up to kilometre level, the tune shifts due to a gradient error would be correspondingly large potentially driving the particles onto a resonance. In addition, as discussed in the Chapter I.8 on transverse linear imperfections, a second consequence of gradient errors is the modulation of the betatron amplitude, known as *beta beat*

$$\frac{\Delta\beta(s)}{\beta(s)} = -\frac{1}{2\sin 2\pi Q}\int_s^{s+C} \beta(\tilde{s})\Delta k_1(\tilde{s})\,\cos\{2(\psi(\tilde{s}-\psi(s)) - 2\pi Q)\}\,\mathrm{d}\tilde{s}. \tag{I.14.62}$$

Equation (I.14.62) clearly shows that both the quadrupole gradient $\Delta k_1(\tilde{s})$ and β-function $\beta(\tilde{s})$ at the position of the perturbed quadrupole drive the amplitude of the modulation. Since both of these factors are very large, the resulting effect is significant.

Finally, the alignment of the final focus quadrupoles needs to be of highest precision. If the quadrupoles are installed with a transverse offset Δx, their field can be decomposed into the sum of a quadrupole field depending on x and a constant dipole field

$$\frac{e}{p}B_y = k_1(x+\Delta x) = k_1 x + \underbrace{k_1\Delta x}_{\Delta k_0}. \tag{I.14.63}$$

The additional dipole component $\Delta k_0 = k_1\Delta x$ affects the closed orbit given by

$$CO(s) = \frac{\sqrt{\beta(s)}}{2\sin\pi Q}\oint(-\Delta k_0(\tilde{s}))\sqrt{\beta(\tilde{s})}\cos(|\phi(\tilde{s})-\phi(s)| - \pi Q)\,\mathrm{d}\tilde{s}. \tag{I.14.64}$$

The closed orbit distortion is determined not only by the size of the misalignment but also by the large quadrupole strength and the large value of the beta function at the location of the quadrupole $\beta(\tilde{s})$. When examining the closed orbit distortion at the position of the quadrupole, i. e. for the case $s = \tilde{s}$, the effect becomes even more pronounced, as $CO(s)$ is proportional to $\beta(\tilde{s})$ rather than $\sqrt{\beta(\tilde{s})}$.

In summary, the final focus quadrupoles must be both strong and provide a large aperture. Their magnetic field must be extremely precise and stable, and they must be installed with the highest precision.

I.14.10.6 I heard of "local chromaticity correction" – what is that?

The strive for highest luminosities leads to values of β^* approaching the millimetre range. Correspondingly, as a direct consequence of Liouville's theorem, one finds extremely divergent beams leading to β-functions of several kilometres. Recalling the equation for the chromaticity (see Chapter I.3 on transverse beam dynamics),

$$\frac{\mathrm{d}Q}{\mathrm{d}\delta} = -\frac{1}{4\pi}\int \beta(s)k_1(s)\,\mathrm{d}s, \tag{I.14.65}$$

the contribution to chromaticity is proportional to the strength of the quadrupoles k_1 and the value of the β-function at their location. The squeezing of the beams to a small β^* requires the strongest quadrupoles in the lattice. In addition, in the final focus quadrupoles the β-functions reach their maximum values, which means they have the largest contribution to chromaticity exceeding the contribution of all quadrupoles in the rest of the lattice combined. At SUPER-KEK-B, about $80\,\%$ of the chromaticity is created by the final focus quadrupoles [47]. The idea is therefore to correct it as close to the source as possible, at best "locally" in the interaction region.

Local chromaticity correction has been developed in the context of linear colliders. In general, the sextupoles have to be installed in dispersive sections of the lattice to correct for chromaticity. In linear colliders without transverse deflection, no dispersion is created and, thus, the chromaticity created by the quadrupoles cannot be corrected. Therefore, an additional section has been included in the interaction region, where dipoles locally create dispersion so that pairs of identical sextupoles can correct chromaticity before the beams are collided. In modern circular colliders the concept of local chromaticity correction has been adopted, especially for electron-positron colliders such as Higgs and B factories. An example of such an interaction region with local chromaticity correction is presented in Fig. I.14.31 [5], which shows lattice and optics of the interaction region proposed for the FCC-ee. The layout is asymmetric, designed to minimise the synchrotron radiation towards the interaction point located at $s = 0$. The beam passes from left to right through a section of dipole magnets that create dispersion – in this plot denoted as η. The sextupoles of the local chromaticity correction scheme are installed at the positions (a)-(d). The sextupoles at (a) and (d) are additionally used to implement the crab-waist collision scheme that has been mentioned in Sec. I.14.10.2.

I.14.11 Summary

What appears straightforward in this chapter is, in reality, only a first glimpse into the complexities of accelerator design. Particularly for large-scale projects, the design phase can span several years or even decades. This chapter aims to provide guidelines for compiling a list of beam parameters and the resulting fundamental layout decisions. In addition, a step-by-step approach has been presented for constructing an initial lattice of a circular collider. In fact, this very approach has been applied for the first lattice design of FCC-ee [12]. The subsequent work by numerous expert groups extends beyond the scope of this discussion. Specifically, this involves studies on the effects of imperfections, such as magnet misalignments, or how collective effects compromise beam stability. Both areas require complex particle tracking studies. Additionally, sections dedicated to injection, extraction, beam collimation, and beam dumps must be designed. Depending on the specific laboratory, an injector or even an injector chain has to be designed and built that require their own accelerator design. As mentioned in the in-

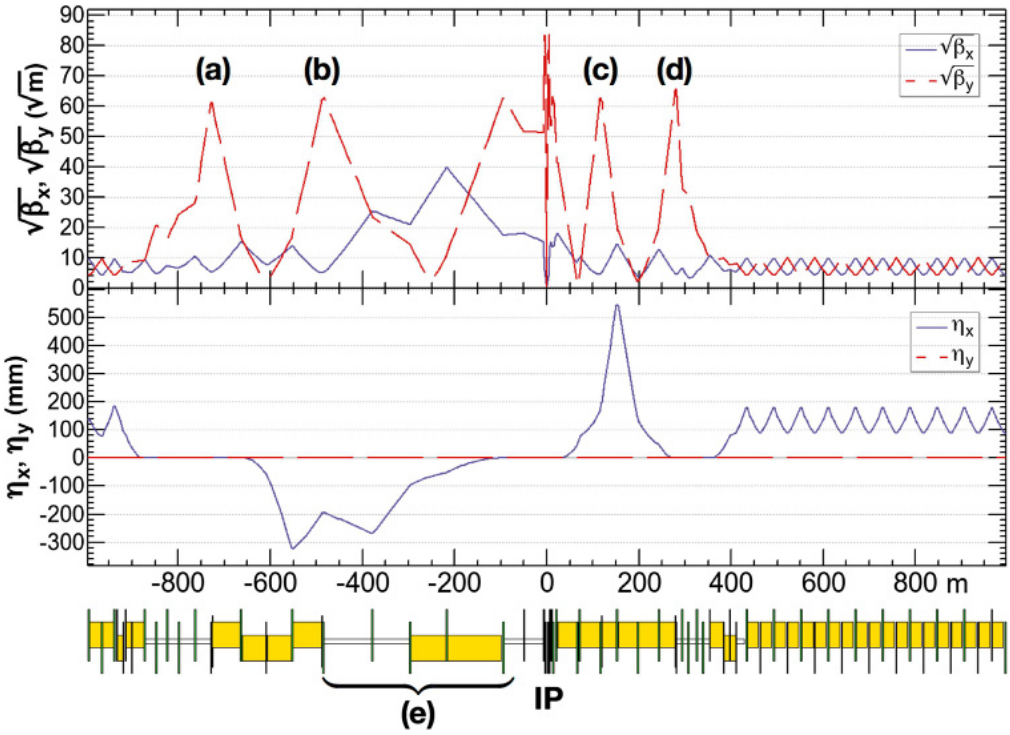

Fig. I.14.31: The beam optics of the FCC-ee interaction region for $t\bar{t}$ operation as proposed in the Conceptual Design Report [5]. The upper plot shows the square roots of the $beta$-functions, the lower plot the dispersion functions, which in this plot are denoted as η. The beam passes from the left to the right, the interaction point is located at $s = 0$. The layout of the interaction region is asymmetric to suppress synchrotron radiation towards the interaction point. The critical energy of the synchrotron radiation created by the dipoles in region (e) is below $100\,\mathrm{keV}$. The dipoles are used to create dispersion for the sextupoles of the local chromaticity correction scheme, which are located at positions (a)-(d). The sextupoles at (a) and (d) are additionally used to implement the crab-waist scheme.

troduction, various hardware systems need to be designed, including magnets, vacuum and RF systems, and beam diagnostics. Finally, engineering challenges, encompassing civil engineering, power concepts, surveying, and personnel safety systems, etc. must be investigated and resolved...

... and then you just turn the key and run the machine.

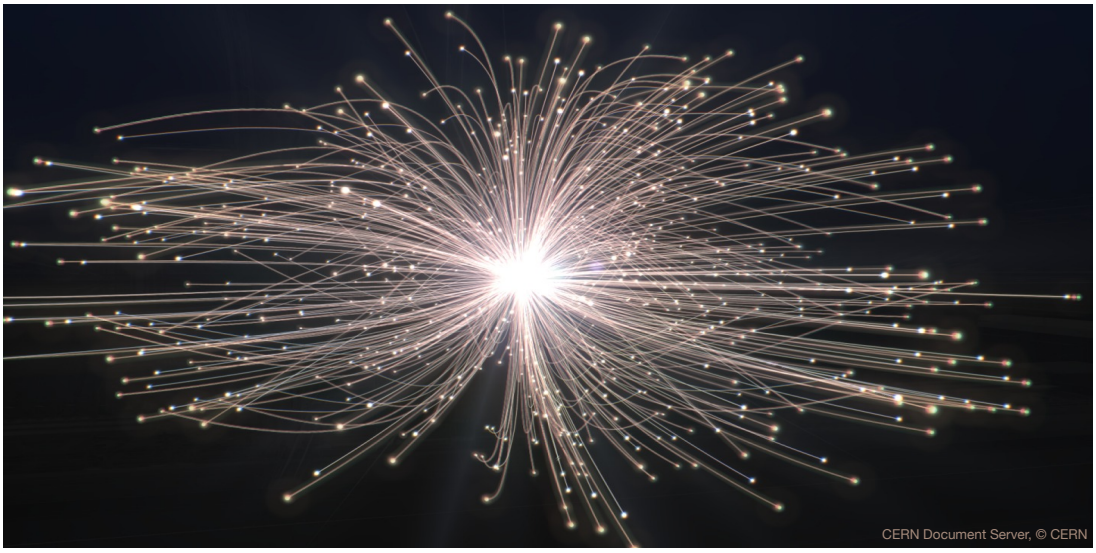

JUAS'24 Accelerator Design Workshop: Exercises

Tutors: Kevin André, Bastian Härer, Bernhard Holzer, Carsten Mai, Adrian Oeftiger

February 2024

1 Timetable

JUAS slots with lectures introducing the mini-workshop:

- Tuesday, 6 February, 9:00 to 12:00
- Wednesday, 7 February, 16:00 to 18:00

JUAS slots to work on exercise set:

- Thursday, 8 February, 16:00 to 18:00
- Friday, 9 February, 9:00 to 12:00 and 14:50 to 17:50
- Monday, 12 February, 9:00 to 12:00

$\Longrightarrow$ finish presentation slides for your group until the exam.

Exam: marked 9-minute presentations follow during the day on Tuesday, 13 February (schedule as announced on indico). Every group will present their results to the jury and answer questions. Make sure that every group member presents a fair share. Prepare the slides such that the other students working on different aspects of the machine can comprehend: selected groups will repeat their presentation during the workshop conclusion (Tuesday, 13 February at 14:30).

2 Introduction

The goal of the accelerator design workshop is to apply the knowledge gained during this school to a realistic study case. The task is to design a particle accelerator with certain specifications and boundary conditions. The idea is to gain experience how such a big task is tackled and organised. There are eight groups of three or four students each. We assigned three topics, each treats the same problem from a slightly different angle and with different emphasis.

Scope: design a top factory for precision measurements. Design a particle collider for precision measurements of the top quark mass at the $t\bar{t}$-threshold. The circumference must not exceed 100 km and the maximum synchrotron radiation power is limited to 50 MW *per beam*. Per year at least 100 000 $t\bar{t}$ pairs should be produced for sufficient experiment statistics.

3 Topic I: Basic parameter set and general design aspects

Develop a basic parameter set for the machine and determine general design aspects.

3.1 Overview

- Energy, cross section, luminosity
- No. of bunches, particles per bunch, β^* and emittance
- General layout, arcs and straight sections, magnet technology, focusing cell layout and dipole filling factor
- Synchrotron radiation power, resistive wall impedance induced power loss

3.2 Boundary Conditions

1. Maximum circumference: 100 km
2. Maximum synchrotron radiation power per beam: 50 MW
3. Number of events per year: 100 000
4. Number of experiments: 2

3.3 Exercises

1. Why would we choose to collide electrons and positrons instead of protons?
2. The most important parameter for your particle collider is its luminosity. What beam energy is optimal for $t\bar{t}$-production? Think about the effective running time of the collider per year and consider the cross section at this beam energy (use "Bare TOPPIK" computation). What average instantaneous luminosity is required to obtain 100 000 number of events per year? (Consider the luminosity to be constant during the run.)

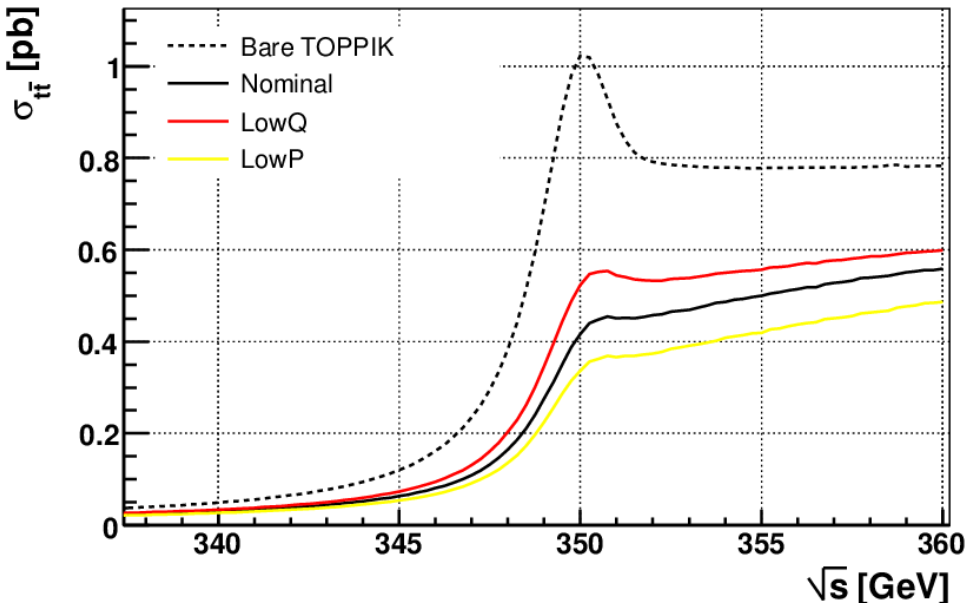

Figure 1: Cross section for $t\bar{t}$-production in electron-positron collisions[1]

3. Consider e.g. the FCC-ee, where the interaction point beam sizes are of the order $\sigma_x^* \approx 50\,\mu\text{m}$ and $\sigma_y^* \approx 50\,\text{nm}$. How much beam current do you need for the previously computed luminosity? How many bunches N_b do you accommodate per beam? What is the bunch population figure (N_p, number of particles per bunch)?

4. Estimate reasonable values for the transverse rms emittances via discussing with your colleagues (groups working on the lattice design topic III). Comment on the ratio between horizontal and vertical emittance.

5. Define the requirements for the interaction region: what β^* do you need? What consequences does this have for the distance to the final focusing system, L^*, as well as the beam size figures there?

6. Think about a machine layout: What percentage of the ring consists of arc and straight sections? How many straight sections do you include and for which purposes?

7. Outline a layout for your basic cell. What cell type would you use and why?

8. Estimate the dipole filling factor in the machine. What is the local bending radius ρ? Please justify which magnet technology you would use – normal-conducting or superconducting?

9. Do you plan for one or two beam pipes? What are the consequences and limitations?

10. Check the feasibility of your parameters by estimating the expected synchrotron radiation power P_{SR}. Where would you adjust your parameter set to reach lower P_{SR} figures?

11. If time permits: impedance induced energy loss.

    (a) Another source of beam energy loss is given by the resistive wall impedance of the machine. Consider a beam of N_b Gaussian-distributed bunches of rms length σ_z with N_p particles of charge e travelling inside a vacuum tube of radius r_p made of copper (with a conductivity of $\sigma_c \approx 6 \times 10^7\,\text{S/m}$). In the resistive vacuum tube walls the beam loses a power figure of

    $$P_{RWI} = \frac{N_b\,(e\,N_p)^2}{T_0}\,k_{||} \tag{1}$$

    with T_0 the revolution period. The loss factor per circumference C is given by

    $$\frac{k_{||}}{C} = \frac{1.225c}{4\pi^2 r_p {\sigma_z}^{3/2}}\sqrt{\frac{Z_0}{2\sigma_c}} \quad , \tag{2}$$

    where c denotes the speed of light and Z_0 the vacuum impedance.

    Estimate the corresponding impedance related total power loss for our two colliding beams. For the equilibrium σ_z figure you can refer to your colleagues (groups working on the synchrotron radiation topic II).

    Compare the P_{RWI} figure to the synchrotron radiation induced power loss P_{SR} you computed before.

    (b) Consider exploiting your designed machine also to study weak neutral current interactions around the Z pole at a centre-of-mass energy of $\sqrt{s} \approx 91\,\text{GeV}$. What would be the corresponding emitted synchrotron radiation power P_{SR} per beam?

    Imagine hypothetically increasing the number of bunches N_b until the machine is filled with bunches[1] spaced at 25 ns, leaving an abort gap of 10%. How does P_{SR} compare to the resistive wall impedance related P_{RWI} now?

    This might give you a feeling for the relevance of collective effects for constraining the beam and bunch parameters.

[1] Juste, Aurelio et al., "Determination of the top quark mass circa 2013: methods, subtleties, perspectives", The European Physical Journal C, vol. 74, Oct. 2014

[1] This is of course unrealistic: collective effects such as single- and coupled-bunch instabilities as well as residual gas interaction (fast beam-ion and electron cloud instabilities) pose more stringent limits to N_b (also dedicated beam filling schemes) and N_p.

4 Topic II: Synchrotron radiation emissions and Radio-Frequency sections

4.1 Exercise summary

1. SR power, critical energy, beam current and comparison to proton particles
2. Momentum compaction factor, transition energy, RF voltage, synchronous phase
3. Number of RF cavities and length of the RF section, synchrotron tune, RF acceptance
4. Damping times, equilibrium emittance, energy spread and bunch length
5. Dipole length for $\Phi_{x,y}$=60° or 90°, FODO cell length

4.2 Exercises

1. Geometry assumptions: the ring has four straight sections with two interaction regions, one RF section and one injection section. You will design a lepton collider with a beam energy of 175 GeV. In this study, you will assume a circumference of 100 km and consider a bending radius $\rho = 10.0$ km ($\approx 63\%$ of the ring is composed with dipole magnets).
   (a) Compute the beam current in order to reach 50 MW power lost per beam due to synchrotron radiation. Estimate a number of bunches from the number of particles you obtain with the beam current. You can discuss the results with your colleagues from Topic I.
   (b) Compute the associated critical energy and energy loss per turn.
   (c) Find the required cooling per arc using the line power density, assuming the arcs represent 80% of the total circumference. For your information LEP had a cooling capability of 1.1 kW/m, will your machine need more ?
   (d) What proton beam energy could the same storage ring circumference handle assuming 0.06% of the FCC-ee energy loss ? What would need to be modified to operate with proton beams ?

	Unit	**LEP**	**LHC**	**FCC-ee**	**FCC-hh**
Beam particle		e+/e-	p	e+/e-	p
Circumference	km	26.7	26.7	97.8	97.8
Beam energy	TeV	0.1	7.0	0.1825	50.0
Beam current	A	0.006	0.54	0.0064	0.5
Energy loss per turn	MeV	2800	5.890	9200	4.670
Critical energy	keV	700	0.044	1060	4.3
SR power	kW	1.7×10^4	7.5	1.0×10^5	4.8×10^3

Table 1: From: O. Grobner CERN-LHC/VAC VLHC Workshop Sept. 2008 and FCC-ee CDR.

2. The orbit length fluctuation with the energy offset is proportional to the momentum compaction factor. The momentum compaction factor is a property of the lattice and is assumed to be 7.3×10^{-6}.

   (a) What is the transition energy ? Are we below or above transition ? Deduce the synchrotron phase.

   (b) What total RF voltage is required to compensate the energy loss per turn ? Are we in an acceleration or a stationary regime ? In order to have a stable phase, one needs to operate the RF cavities off-crest so that the electron beam can be stored for many revolutions in the storage ring. The cavity phase is set to 110°, re-compute the total RF voltage required, assuming an RF frequency of 400 MHz.

   (c) Compute the synchrotron tune and compare it to the transverse tune and to the revolution period.

   (d) What type of RF cavities would you use? Given the RF cavity provide the energy restored by a single RF cavity. How many cavities are needed to restore the energy lost for both counter-rotating beams ? How could you reduce the number of RF cavities ?

   (e) Estimate the straight section length required for the RF cavities assuming that a cryomodule is composed of four RF cavities and measures 7 m (one adds 20% for the other magnetic elements and connections).

   (f) Compute the RF energy acceptance or bucket height. It is common to have an RF energy acceptance of more than ±3 %, how would you achieve it ? What are the implications ?

3. We will now focus on the equilibrium beam parameters.

   (a) Compute the damping times for both transverse and longitudinal planes, and compare to the revolution period, conclusion ? How many turns are needed to reach the steady state ?

   (b) Compute the equilibrium energy spread. Which parameters could we adjust to tune it ?

   (c) Compute the equilibrium bunch length. How many bunches fit in the ring ? To be realistic one can consider a bunch spacing of 25 ns like in the LHC. How many bunches fit into the ring with a 25 ns bunch spacing ? Using 1.a) compute the resulting bunch spacing.

4. If time permits: the arc lattice and its properties.

   (a) Estimate a reasonable value for the horizontal rms emittance via discussing with your colleagues (groups working on the lattice design topic III). Compute the average dispersion function from this equilibrium emittance. Typically, electron storage rings have a phase advance of 60° or 90°. Assuming the magnetic periodic arc structure is a FODO cell, from the average $\mathcal{H}$-function find the dipole magnetic length.

$$\text{For } 60^\circ \text{ phase advance the formula is: } \langle \mathcal{H} \rangle = \frac{15}{2} \frac{L^3}{\rho^2} \tag{3}$$

$$\text{For } 90^\circ \text{ phase advance the formula is: } \langle \mathcal{H} \rangle = \frac{5}{2} \frac{L^3}{\rho^2} \tag{4}$$

   (b) The dipole filling factor is about 80% for the FODO cell, conclude on the FODO cell length. Estimate the number of FODO cells and main dipole magnets (2 dipoles per cell).

5 Topic III: Lattice Design

5.1 Exercise summary

1. Design basic cell according to beam requirements
2. Implement a MAD-X model of your basic cell, close the ring and calculate SR integrals and equilibrium beam parameters
3. Include dispersion suppressors and straight sections to your model and match optics
4. Optional: include RF cavities and calculate equilibrium beam parameters with MAD-X

5.2 Boundary Conditions

1. Damping partition number: $J_x = 1$
2. A maximum circumference of 100 km
3. Maximum synchrotron radiation power: $P = 50\,\mathrm{MW}$ per beam
4. The basic cell should have about the same phase advance in both planes.

Jupyter notebook

5.3 Exercises

This group focuses on the lattice design of a new accelerator. A lattice is being developed to match a pre-defined set of requirements.

1. Design of basic arc cell
   (a) What lattice type do you choose for your basic cell, and why?
   (b) What phase advance per cell do you choose, and why?
   (c) Think about the layout of your basic cell: cell length, length of magnetic elements, dipole filling factor. *Hint:* Start with a cell length of 50 m. You should obtain a dipole filling factor of about 80%.
   (d) Calculate the equilibrium emittance of your lattice. You will need the beam energy, which you can discuss with your colleagues from Topic I. The equilibrium emittance can be approximately calculated using following equation:

$$\epsilon_x = \frac{C_\mathrm{q}}{J_x}\gamma^2\theta^3 F \tag{5}$$

   $C_\mathrm{q} = \frac{55}{32\sqrt{3}}\frac{\hbar c}{m_0 c^2} = 3.832 \times 10^{-13}\,\mathrm{m}$, $J_x \approx 1$ is the damping partition number, γ the Lorentz factor (based on the beam energy), and θ the bending angle of all dipole magnets in a half-cell. For a FODO cell with phase advance μ the factor F can be written as

$$F_\mathrm{FODO} = \frac{1}{2\sin\mu}\frac{5+3\cos\mu}{1-\cos\mu}\frac{L}{l_\mathrm{B}}. \tag{6}$$

   L is the cell length and l_b is the length of all dipole magnets in the cell.
   Calculate the bending radius and bending angle of the dipoles assuming 80% of your lattice is filled with arc cells and 20% with straight sections.
   (e) Calculate the quadrupole strength k_1 using

$$\sin\left(\frac{\mu}{2}\right) = \frac{L}{4f} \qquad \text{and} \qquad \frac{1}{f} = k_1 L_Q \tag{7}$$

   where L_Q is the length of the quadrupole magnets.

(f) Define the elements and the basic cell in MAD-X. Ask your colleagues from topic I to indicate which beam energy you should design for. Set up an MAD-X environment (define beam etc.) and implement your basic cell using thick lenses. Advice: Use sequences, not lines! Check the tunes in the TWISS summary table. Do they fit your expectation?

(g) Match the phase advance of your basic arc cell. Compare the maximum and minimum values of beta functions and dispersion of MAD-X to the analytically calculated values.

(h) Match the chromaticity of your basic arc cell to zero. Can you explain why the sextupole strengths for the "defocusing" sextupole are larger than for the "focusing" one?

(i) Build a full ring with your basic cells. How many cells do you need to close the ring? Do the tunes fit your expectation? Check if the ring is closed (`SURVEY` command).

```
survey;
value, table(survey,yourSequence$END,theta);
```

(j) Calculate the synchrotron radiation integrals (`TWISS, chrom;`). Proceed to calculate equilibrium emittance and energy loss per turn and compare to the requirements.

2. Dispersion suppressors and straight sections

(a) Design a dispersion suppressor section for your storage ring and implement it in MAD-X. What scheme do you use and why? Why is it not possible to use the identical section on both sides of an arc?

(b) Define a straight cell for the straight sections.

(c) Define matching sections for the beginning ("MSL") and the end ("MSR") of your straight sections. Why do you need matching sections? How many parameters do you need to match? How many degrees of freedoms (=quadrupoles) do you need? Match the optics.

(d) Include straight sections at four places in your ring.

(e) Observe tunes and chromaticities. Do they match your expectation? Re-match tunes and chromaticities.

(f) Calculate and save the synchrotron radiation integrals of your storage ring for analytical calculations later.

3. If time permits: RF sections

(a) Estimate the total RF voltage which is needed to compensate the synchrotron radiation energy loss. The energy gain in the cavity is given by

$$U = eV_{\mathrm{RF}} \sin\left(2\pi(\phi - hf_0 t)\right), \tag{8}$$

where ϕ is the phase lag ("synchronous phase"), h the harmonic number of the ring, and f_0 the cavity frequency.

(b) Define a straight cell and straight section that contains RF cavities.

(c) Switch on radiation and observe tunes and chromaticities. Can you explain what happens?

(d) Observe the transverse orbit. Can you explain the pattern you see?

(e) Calculate equilibrium beam parameters with the MAD-X `EMIT` command and compare them to the analytical values from the calculation using the synchrotron radiation integrals calculated above.

(f) How many particles and bunches can you fill into the rings before you reach the limit of synchrotron radiation power?

I.14.12 Answers to the questions

Answer to question I.14.1: Muons carry an approximately two hundred-fold rest mass compared to electrons (and positrons). At a given centre-of-mass energy, a muon collider would correspondingly require much lower kinetic energies compared to an electron-positron collider. This significantly reduces the radiation loss (the power of which scales with the energy to the fourth power) and, consequently, enables the construction of circular colliders which are much smaller in circumference compared to an equivalent electron-positron collider. A major challenge of muon-beam production, though, is given by the short lifetime before the muons decay.

Answer to question I.14.2: When beams share a vacuum chamber, they encounter the same magnetic fields. Due to their opposite charges, electrons and positrons are both deflected towards the ring center when passing through a dipole magnet in opposite directions. Conversely, proton beams in the LHC, having the same charge, would be deflected in opposite directions – one towards the inside and one towards the outside. Thus, opposite dipole fields are essential which requires separate beam pipes.

Sharing a beam pipe is feasible only if the particles in beam 1 are the antiparticles of those in beam 2. When colliding different particle species, such as electrons and protons, or when beams have different energies as seen in B factories, individual vacuum chambers become necessary. Additionally, double-ring colliders achieve higher luminosity as in single-ring colliders, the number of bunches must be kept low to avoid parasitic crossings.

Answer to question I.14.3: For two proton beams in collision, $\sqrt{s} = 2E$. For $\sqrt{s} = 200\,\mathrm{GeV}$, two $100\,\mathrm{GeV}$ proton beams are needed. In fixed-target geometry, $\sqrt{s} = \sqrt{2m^2 + 2Em} \Rightarrow E = [(\sqrt{s})^2 - 2m^2]/(2m)$. In this case a proton beam energy of $21\,321\,\mathrm{GeV}$ is required. The collider geometry is obviously preferable.

Answer to question I.14.4: The synchrotron radiation losses per particle increase $\propto \gamma^4$. In order to maintain the overall budget of $50\,\mathrm{MW/beam}$, the number of bunches has to be reduced, which leads to lower luminosity. While the beams at $45.6\,\mathrm{GeV}$ consist of 16640 bunches, only 48 bunches can be stored at $182.5\,\mathrm{GeV}$ leading to a luminosity reduction from $\mathcal{L} = 460 \times 10^{11}\,\mathrm{cm\,s^{-2}}$ to $\mathcal{L} = 3.1 \times 10^{11}\,\mathrm{cm\,s^{-2}}$.

Answer to question I.14.5:

$$\frac{p_0}{e} = \frac{BNL_\mathrm{B}}{2\pi} \Rightarrow p_0 = \frac{8.3\,\mathrm{T} \cdot 1232 \cdot 14.3\,\mathrm{m}}{2\pi} \cdot 3 \times 10^8\,\mathrm{m\,s^{-1}} \cdot \frac{e}{c} = 6.98\,\mathrm{TeV/c}. \tag{I.14.66}$$

The maximum momentum of the protons in LHC is $6.98\,\mathrm{TeV/c}$.

Answer to question I.14.6: The magnetic field strength of the bending magnets can be calculated using the beam rigidity expression

$$B\rho = \frac{p}{e} \Rightarrow B = \frac{E}{ec\rho} = \frac{182.5\,\mathrm{GeV}}{3 \times 10^8\,\mathrm{m\,s^{-1}} 10.760\,\mathrm{km\,e}} = 56.5\,\mathrm{mT}. \tag{I.14.67}$$

For the example of the lepton collider FCC-ee, normal-conducting magnet technology is foreseen for the bending magnets.

Answer to question I.14.7: The calculations of Eq. (I.14.6) and MAD-X agree well: $\hat{\beta} = 182.5\,\mathrm{m}$ and $\check{\beta} = 31.3\,\mathrm{m}$.

Answer to question I.14.8: After passing the sextupole, the particle motion is defined by

$$x_1 = x_0 \qquad y_1 = y_0$$
$$x_1' = x_0' - \frac{k_2 L_\mathrm{S}}{2}\,(x_0^2 - y_0^2) \qquad y_1' = y_0' - k_2 L_\mathrm{S}\, x_0\, y_0.$$

After the $-I$ transformation the particle arrives at the second sextupole with

$$x_2 = -x_1 = -x_0 \qquad y_2 = -y_1 = -y_0$$
$$x_2' = -x_1' = -x_0' + \frac{k_2 L_\mathrm{S}}{2}\,(x_0^2 - y_0^2) \qquad y_2' = -y_1' = -y_0' + k_2 L_\mathrm{S}\, x_0\, y_0.$$

Since $x_2 = -x_0$ and $y_2 = -y_0$, the second sextupole applies a kick of equal strength, which cancels the additional transverse momentum created by the first sextupole

$$x_3 = x_2 = -x_0 \qquad y_3 = y_2 = -y_0$$
$$x_3' = x_2' - \frac{k_2 L_\mathrm{S}}{2}\,(x_2^2 - y_2^2) = -x_0' \qquad y_3' = y_2' - k_2 L_\mathrm{S}\, x_2\, y_2 = -y_0'.$$

Answer to question I.14.9: The Lorentz factor is $\gamma = E/E_0 = 3.57 \times 10^5$. With a dipole filling factor of $L_\mathrm{B}/L = 0.8$, the bending angle per half-cell is $\theta = 1.87\,\mathrm{mrad}$. 1680 cells are needed to close the ring leading to an arc length of $84\,\mathrm{km}$. Yes, these are realistic design parameters taken from the FCC-ee Study.

Answer to question I.14.10: In order to achieve low or even negative momentum compaction factors the strength of the centre quadrupole has to be increased. This stretches the dispersion function and pushes its periodic solution to negative values at the beginning and at the end of the cell. This adds a negative contribution to the $\mathcal{I}_1$ integral and thus to a low or even negative value of the momentum compaction factor.

Answer to question I.14.11: The solution on the rising edge of the sine wave is used below transition energy, i.e. as long as the particle is non-relativistic, or with negative momentum compaction factor. The solution on the falling edge is used for relativistic beams in storage rings with positive momentum compaction factor, which is the common case.

Answer to question I.14.12: There are two reasons in fact. First, larger beam size reduces brilliance

$$B(\lambda) = \frac{F(\lambda)}{(2\pi)^2 \sigma_x \sigma_{x'} \sigma_y \sigma_{y'}} \propto \frac{1}{\epsilon_x \epsilon_y}.$$

Second, dispersion in insertion devices creates transverse oscillation due to the energy loss and depending on the magnetic field to emittance increase because of the contribution to $\mathcal{I}_5$.

Answer to question I.14.13: In fact, there is no difference. The quadrupole-based dispersion suppressor is nothing else than a matching section specifically used to suppress the dispersion function and re-match the optics.

Answer to question I.14.14: At the LHC, the final focus triplet is shared by both beams. Since the protons have same charge but travel in opposite direction, the quadrupoles have opposite focusing properties for the two beams. If the two beams had opposite charge as in an electron-positron collider, the optics would be symmetric. In the case of HERA, individual quadrupoles were needed for protons and electrons because of the different beam energies and the optics was laid-out symmetrically.

Answer to question I.14.15: In case of flat beams, where the vertical emittance is in the percent or per mille range of the horizontal one, a doublet is used. The quadrupole closer to the interaction point focuses the vertically, the second the horizontally. If the beams are round in the sense that the emittances are similar in both planes, a triplet has better focusing properties.

Answer to question I.14.16: Since particle trajectory and beam size is given by $x(s) = \sqrt{\epsilon\beta(s)}\,\sin(\psi(s)+\psi_0)$ and $\sigma(s) = \sqrt{\epsilon\beta(s)}$, respectively, a quadratic increase of the β-function results in a linear increase of transverse offset and beam size, as expected from free propagation in a drift space.

Acknowledgements

We would like to thank Bernhard Holzer, who has taught the accelerator design workshop before and provided a lot of teaching material, experience and wisdom. Big thanks also to Kevin André and Carsten Mai for their contribution to the design of the exercises and their continuous enthusiastic supervision of the student teams during the workshop each year at JUAS.

References

[1] A. Oeftiger *et al.*, Joint Universities Accelerator School 2024: Accelerator design workshop—notebook for lattice design, 2024, Zenodo, doi:10.5281/zenodo.10877903.

[2] CMS Collaboration, Displays of events from Run 3 seen in CMS with multiple reconstructed vertices, 2023, CERN Document Server.

[3] CERN Photolab, "OPAL event on display", 1989, CERN Document Server.

[4] Future Circular Collider Study, Volume 1: Physics Opportunities. Conceptual Design Report, preprint edited by M. Mangano *et al.* CERN accelerator reports, CERN-ACC-2018-0056 (CERN, Geneva, 2018), published in *Eur. Phys. J. C* **79** (2019) 474, doi:10.1140/epjc/s10052-019-6904-3.

[5] Future Circular Collider Study, Volume 2: The Lepton Collider (FCC-ee) Conceptual Design Report, preprint edited by M. Benedikt *et al.* CERN accelerator reports, CERN-ACC-2018-0057 (CERN, Geneva, 2018), published in *Eur. Phys. J. Spec. Top.* **228** (2019) 261–623 , doi:10.1140/epjst/e2019-900045-4.

[6] R. Schmidt *et.al.*, Protection of the CERN Large Hadron Collider, *New Journal of Physics* **8** (2006) 290, doi:10.1088/1367-2630/8/11/290.

[7] P.J. Bryant, K. Johnsen, *The principles of circular accelerators and storage rings*, Cambridge University Press, 1993, doi:10.1017/CBO9780511563959.

[8] A. Wolski, *Beam Dynamics in High Energy Particle Accelerators*, Imperial College Press, 2014, doi:10.1142/p899.

[9] B.J. Holzer, Lattice design in high-energy particle accelerators, in : *CAS - CERN Acceleration School: Intermediate accelerator physics*, CERN-2006-002 (CERN, Geneva, 2006), pp. 31-74 doi:10.5170/CERN-2006-002.31.

[10] B.J. Holzer, Lattice design in high-energy particle accelerators, in: *CAS - CERN Accelerator School: Advanced Accelerator Physics Course*, CERN-2014-009 (CERN, Geneva, 2014), pp. 61-100, doi:10.5170/CERN-2014-009.61.

[11] A. Wolski, Low-emittance Storage Rings, in: *CAS - CERN Accelerator School: Advanced Accelerator Physics*, CERN-2014-009 (CERN, Geneva, 2014), pp. 245–294, doi:10.5170/CERN-2014-009.245.

[12] B. Härer, Lattice design and beam optics calculations for the new large-scale electron-positron collider FCC-ee, doctoral dissertation, Karlsruhe Institute of Technology (KIT), 2017, doi:10.5445/IR/1000071240.

[13] LHC Design Report Vol. 1: The LHC Main Ring, edited by O. Brüning *et al.*, CERN-2004-003-V1 (CERN, Geneva, 2004), doi:10.5170/CERN-2004-003-V-1.

[14] A. S. Langner, A Novel Method and Error Analysis for Beam Optics Measurements and Corrections at the Large Hadron Collider, CERN-THESIS-2016-299, doctoral dissertation, Universität Hamburg, 2017, CERN Document Server.

[15] H. Wiedemann, *Particle accelerator physics*, 4th ed., Springer, 2015, doi:10.1007/978-3-319-18317-6.

[16] A. Bogomyagkov, S. Glukhov, E. Levichev, P. Piminov, Effect of the Sextupole Finite Length on Dynamic Aperture in the Collider Final Focus, arXiv:0909.4872 (2009), doi:10.48550/arXiv.0909.4872.

[17] L.C. Teng, Minimizing the emittance in designing the lattice of an electron storage ring, FERMILAB-TM-1269 (Fermi National Accelerator Lab., Batavia, IL (USA), 1984), doi:10.2172/6690255.

[18] R. Chasman, G.K. Green, E.M. Rowe, Preliminary design of a dedicated synchrotron radiation facility, in *IEEE Transactions on Nuclear Science*, vol.22, no.3, pp. 1765-1767, June 1975 doi:10.1109/TNS.1975.4327987.

[19] A.W. Chao, K.H. Mess, M. Tigner, F. Zimmermann, *Handbook of Accelerator Physics and Engineering*, 2. ed., World Scientific, 2013, doi:10.1142/8543.

[20] L. Farvacque, *et al.*, ESRF accelerator upgrade project status, EuCARD^2 Low Emittance Rings Workshop, Grenoble, France, 2015 Indico.

[21] J. Wenninger *et al.*, Future Circular Collider Study, Lepton Collider Parameters, FCC-1401201640-DSC, Feb. 2014. Indico.

[22] P. Raimondi, The ESRF Low-emittance Upgrade, in *Proc.7th Int. Particle Accelerator Conf. (IPAC'16), Busan, Korea, May 2016*, paper WEXA01, pp. 2023–2027, 2016, doi:10.18429/JACoW-IPAC2016-WEXA01.

[23] Sirius' storage ring parameters, website of the Brazilian Synchrotron Light Laboratory (LNLS).

[24] ESRF-Extremely Brilliant Source parameters, website of the European Synchrotron Radiation Facility (ESRF).

[25] MAX IV 3 GeV storage ring parameters, website of the MAX IV laboratory.

[26] The LEP Energy Working Group, Calibration of centre-of-mass energies at LEP 2 for a precise measurement of the W boson mass, *Eur. Phys. J. C* **39**, 253–292 (2005), doi:10.1140/epjc/s2004-02108-8

[27] F. Peauger, Baseline and Options for FCC-ee SRF Cavities, presentation at the FCC Week 2022, Paris, France, May 2022, Indico.

[28] F. Valchkova-Georgieva, General lay-out, integration update rf systems, presentation at the FCC Week 2023, London, United Kingdom, June 2023, Indico.

[29] P.J. Bryant, Insertions, in: *CAS - CERN Accelerator School: 5th General Accelerator Physics Course*, CERN-1994-001 (CERN, Geneva, 1994), pp. 159–190, doi:10.5170/CERN-1994-001.159.

[30] B. Haerer, T. Tydecks, Lattice Design and Dynamic Aperture Studies for the FCC-ee Top-Up Booster Synchrotron, arXiv:2111.14462 (2021), doi:10.48550/arXiv.2111.14462.

[31] A Multi-TeV Linear Collider Based on CLIC Technology: CLIC Conceptual Design Report, CERN Yellow Reports: Monographs, CERN-2012-007 (CERN, Geneva, 2012), doi:10.5170/CERN-2012-007.

[32] D. Brandt *et al.*. Accelerator Physics at LEP, *Rep. Prog. Phys.* **63** (2000) 939, doi:10.1088/0034-4885/63/6/203.

[33] W. Herr, B. Muratori, Concept of luminosity, in: *CAS - CERN Accelerator School: Intermediate Accelerator Physics*, CERN-2006-002 (CERN, Geneva, 2006), pp. 361–378, doi:10.5170/CERN-2006-002.361.

[34] High-Luminosity Large Hadron Collider (HL-LHC): Technical design report, CERN Yellow Reports: Monographs, CERN-2020-010 (CERN, Geneva, 2020), doi:10.23731/CYRM-2020-0010.

[35] R. B. Palmer, Energy Scaling, Crab Crossing, and the Pair Problem, eConf **C8806271** (1988), 613–619, SLAC-PUB-4707, Inspire.

[36] K. Oide, K. Yokoya, The Crab Crossing Scheme for Storage Ring Colliders, *Phys. Rev. A* **40** (1989) 315–316, doi:10.1103/PhysRevA.40.315.

[37] M. Zobov, Crab Waist collision scheme: a novel approach for particle colliders, *J. Phys.: Conf. Ser.* **747** (2016) 012090, doi:10.1088/1742-6596/747/1/012090.

[38] P. Raimondi, D.N. Shatilov, M. Zobov, Beam-Beam Issues for Colliding Schemes with Large Piwinski Angle and Crabbed Waist, arXiv:physics/0702033 (2007), doi:10.48550/arXiv.physics/0702033.

[39] P. Raimondi, M. Zobov and D. Shatilov, Beam-beam simulations for particle factories with crabbed waist, in 2007 IEEE Particle Accelerator Conference (PAC), Albuquerque, NM, USA, 2007, pp. 1469–1471, doi: 10.1109/PAC.2007.4440792.

[40] M. Zobov, P. Raimondi, D. N. Shatilov, Suppression of Beam-beam Resonances in Crab Waist Collisions, in: *EPAC08 - Proceedings*, 2008, JACoW.

[41] W. Herr and T. Pieloni, Beam-Beam Effects, in: *CAS - CERN Accelerator School: Advanced Accelerator Physics Course*, CERN-2014-009 (CERN, Geneva, 2014), pp. 431–459, doi:10.5170/CERN-2014-009.431.

[42] A. Piwinski, Synchro-betatron resonances, in Proc. *CERN Accelerator School : Accelerator Physics*, CERN-1987-003-V-1 (CERN, Geneva, 1987), pp. 187–202, doi:10.5170/CERN-1987-003-V-1.187.

[43] S. Petracca, K. Hirata, Dispersion in the interaction point, in *Proc. 1997 Particle Accelerator Conference (PAC'97)*, Vancouver, B.C., Canada, 1997, JACoW.

[44] LHC Injectors Upgrade, Technical Design Report - Volume I: Protons, CERN-ACC-2014-0337 (CERN, Geneva, 2014), doi:10.17181/CERN.7NHR.6HGC.

[45] LHC Injectors Upgrade, Technical Design Report - Volume II: Ions, CERN-ACC-2016-0041 (CERN, Geneva, 2016), doi:10.17181/CERN.L6VM.UOMS.

[46] H. Schmickler, Colliders, in : *Proc. CERN–Accelerator–School course: Introduction to Particle Accelerators*, arXiv:2011.01638 (2020), doi:10.48550/arXiv.2011.01638.

[47] Y. Ohnishi, *et. al.*, Accelerator design at SuperKEKB, *Prog. Theor. Exp. Phys.* **2013** (2013) 03A011, doi:10.1093/ptep/pts083.